NASA Contractor Report 2918

Noise Characteristics of Upper Surface Blown Configurations - Summary

N. N. Reddy and J. S. Gibson

CONTRACT NAS1-13870
JUNE 1978

NASA

NASA Contractor Report 2918

Noise Characteristics of Upper Surface Blown Configurations - Summary

N. N. Reddy and J. S. Gibson
Lockheed-Georgia Company
Marietta, Georgia

Prepared for
Langley Research Center
under Contract NAS1-13870

National Aeronautics
and Space Administration

**Scientific and Technical
Information Office**

1978

FOREWORD

This program summary document is one of three reports prepared by the Lockheed-Georgia Company for NASA Langley Research Center under Contract NAS1-13870, "Exploratory Studies of the Noise Characteristics of Upper Surface Blown Configurations." The other two reports under this contract are CR-145143, which covers the detailed experimental program, and CR-2812, which covers the analytical and theoretical program.

CONTENTS

	Page
FOREWORD	iii
INTRODUCTION	1
SYMBOLS	4
FLOW CHARACTERISTICS	7
Flow Visualizations	8
Flow Measurements	12
ACOUSTIC CHARACTERISTICS	17
Parametric Effects	19
Scaling Effects	22
Forward Speed Effects	27
Noise Reduction Techniques	27
Comparison with Other Data	31
Additional Experiments	34
PREDICTION PROGRAM	34
INTEGRATION OF AIRCRAFT NOISE AND PERFORMANCE	36
THEORETICAL DEVELOPMENTS	45
CONCLUSIONS	52
REFERENCES	55

INTRODUCTION

The primary objective of this program was to develop a data base which will provide the technology required for low noise configurations of upper surface blown (USB) propulsive-lift aircraft during takeoff and landing operations. In order to achieve this objective, systematic experimental and analytical investigations were conducted. The overall approach of this program is illustrated in the form of a flow chart in figure 1. The experimental studies were of two types: (1) acoustic characteristics and (2) flow characteristics related to noise generating mechanisms.

Acoustic characteristics were measured in three different facilities. The first was the Anechoic Room where free-field radiated sound was measured on a small scale model to understand noise source characteristics and to establish the effect of various geometric and operating parameters [i.e., nozzle exit geometry and area, nozzle pressure ratio (jet velocity), longitudinal and vertical location of the nozzle on the wing, flap radius of curvature, flap length, and flap deflection angle]. Schematic diagrams of the test configuration are shown in figure 2. An initial series of screening tests determined which produced the most significant noise effects. Then, more detailed investigations were made of the more significant parameters. A second series of tests were conducted in the Acoustic and Performance Facility, where a large-scale model was used to determine the scaling effects of radiated sound, to evaluate surface fluctuating pressures, to evaluate noise reduction concepts, and to measure static aero-propulsive performance. The third set of experiments were conducted in the Acoustic Free-Jet Facility (anechoic open-throat wind tunnel) – to determine forward speed noise effects, near-field noise and aero-propulsive performance.

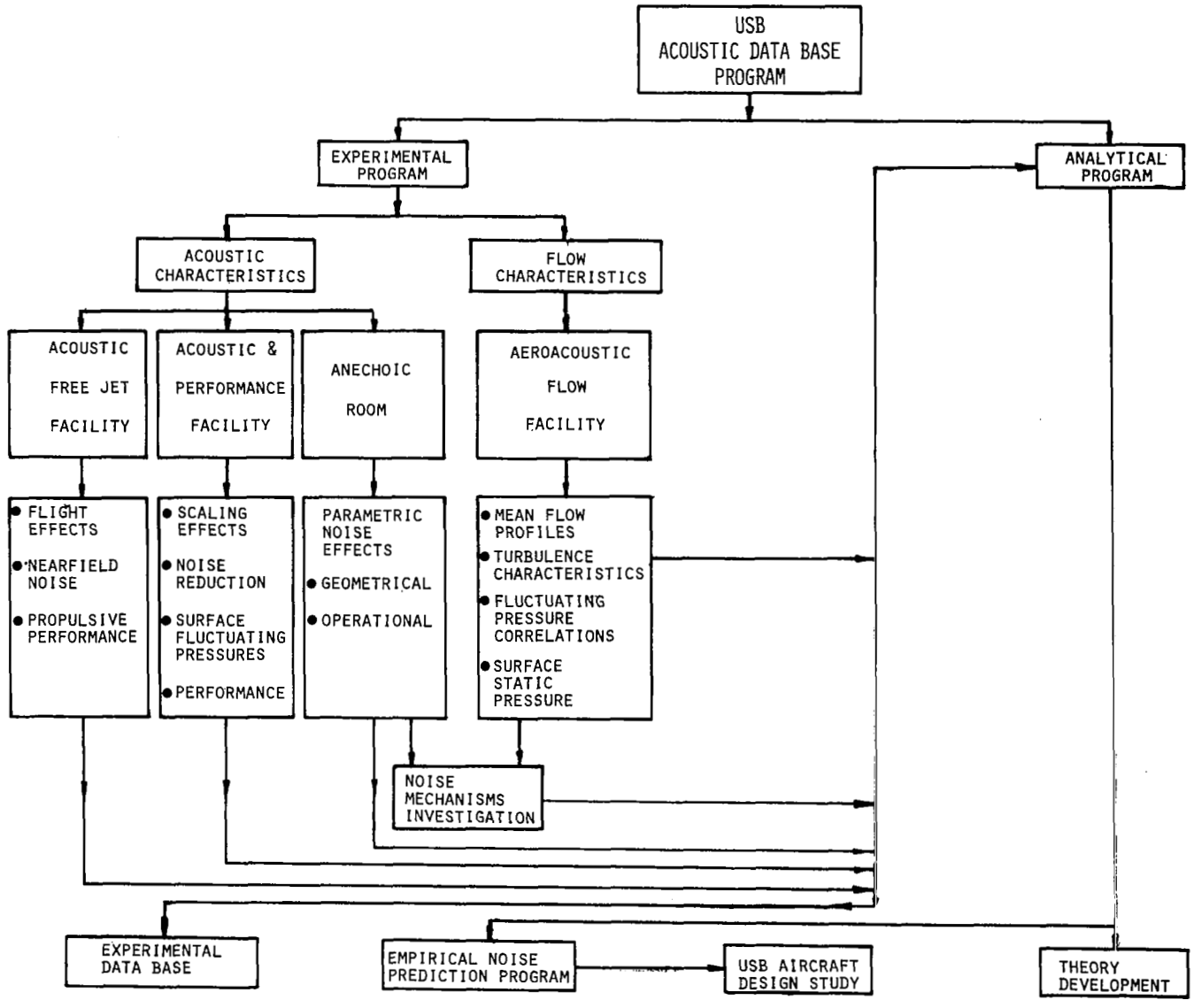

Figure 1. USB Noise Program Outline

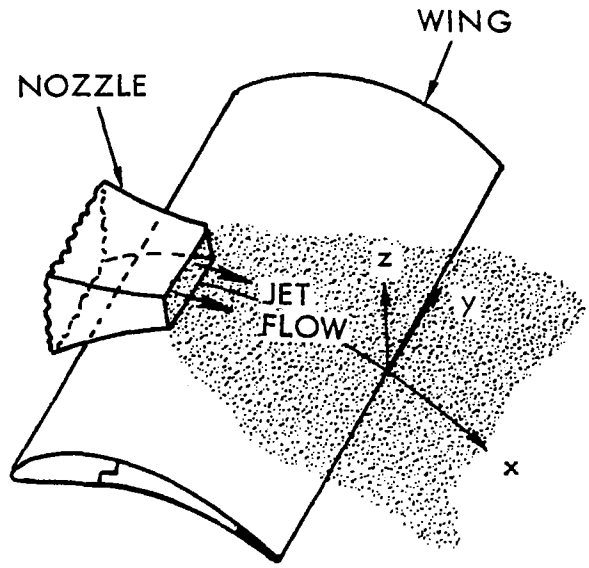

(a) COORDINATE SYSTEM USED IN FLOW AND TURBULENCE MEASUREMENTS

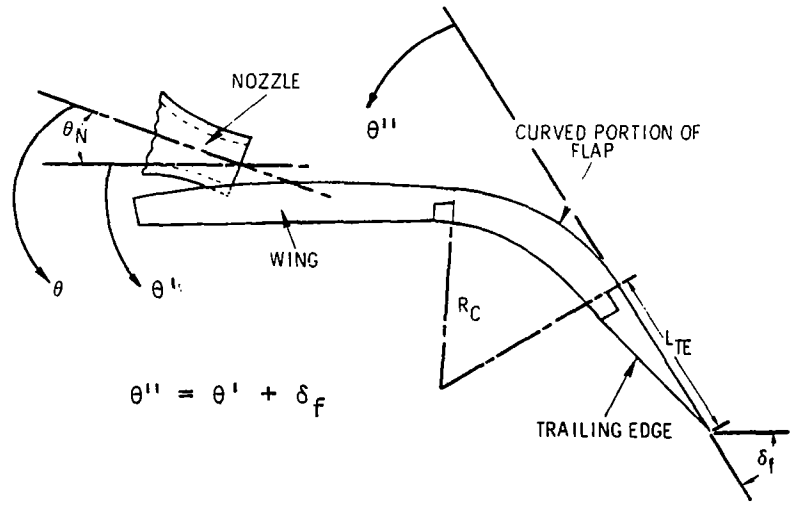

(b) SCHEMATIC DIAGRAM OF EXPERIMENTAL MODEL

Figure 2. Upper Surface Blown Flap Configuration

Flow characteristics were measured primarily in the Aero-Acoustic Flow Facility, using the same small scale model and test parameters as in the Anechoic Room. In addition, space-time correlations of turbulence were measured. Flow visualizations (oil flow and Schlieren techniques) were also conducted in this facility.

The experimental results from all the facilities were used in (1) providing a systematic experimental data base, (2) identifying the dominant noise sources for USB systems, (3) understanding the physics of noise generating processes, and (4) providing the background data and physical insight to aid in developing a meaningful noise theory.

Theoretical methods alone are not yet advanced enough to be capable of predicting USB noise. Therefore, a USB noise prediction program was developed from a rational combination of theory and empirical techniques based on the parametric experimental data base. Finally, the noise prediction program was used in a brief USB aircraft design study to insure compatibility between low noise trends and good aerodynamic performance.

This volume summarizes the results and conclusions of the overall noise technology development program, and includes significant highlights on noise sensitive flow characteristics, experimentally determined acoustic characteristics, the noise prediction program, the aircraft design study, and acoustic theory development.

SYMBOLS

A_i	empirical constants to fit the autocorrelation function of fluctuating velocities
A_N	nozzle exit area
A_O	nozzle exit reference area
AR_N	nozzle aspect ratio
AR-2	rectangular nozzle with aspect ratio of 2
AR-4	rectangular nozzle with aspect ratio of 4

AR-8	rectangular nozzle with aspect ratio of 8
C	function of flow properties (equation 4)
c	wing chord
$D(\psi,\omega)$	directivity of radiated sound
D_H	hydraulic diameter of nozzle exit
f	frequency, Hz
f_c	one-third octave band center frequency, Hz
$G(z',z'')$	lateral space correlation function of fluctuating velocities at zero time delay
H	nozzle exit equivalent height
H_s	height of the trailing edge slot
K	constant (equations 1 and 2)
K_o	modified Bessel function of zeroth order
L_F	flow length (length on the wing and flap surface from the nozzle exit to the trailing edge)
L_{FC}	streamwise length on the flap surface between the start and end of curvature
L_s	effective length of shear layer in the trailing edge wake
L_{TE}	length of the flap between the end of the curvature and the flap trailing edge
L_w	streamwise length of the wing between the nozzle exit and the start of curvature
M	flow Mach number in the trailing edge wake
N	summation number (equation 3)
NPR	Nozzle Pressure Ratio
n	velocity exponent (equations 1 and 2)
QCSEE	Quiet Clean Short-Haul Experimental Engine
R	distance of the noise measurement location from aircraft or experimental model
$R_f(\Delta x,\tau)$	correlation function
R_c	flap knee radius of curvature

R_o	reference distance
S	Strouhal number
U	typical velocity
U_c	eddy convection velocity
u,v,w	longitudinal, lateral, and transverse components (x,y,z) of velocities
$\bar{u},\bar{v},\bar{w}$	mean velocities in the x,y, and z directions
u',v',w'	fluctuating velocities in the x,y, and z directions
V_J	jet exit velocity
V_o	reference velocity
V_{slot}	velocity of trailing edge slot flow
V_T	tunnel flow velocity
W	nozzle exit equivalent width
W_F	flow scrubbed width at the end of curvature of the flap
W_N	flow scrubbed width on the wing at the nozzle exit
W_{TE}	flow scrubbed width at the trailing edge of the flap
W_W	flow scrubbed width at the start of curvature
X,x',x''	longitudinal (streamwise) coordinates
X_N	longitudinal position of the nozzle exit on the wing
X_o	longitudinal location of the fixed hot wire
Δx	longitudinal separation distance between the two hot wires
Y,y',y''	lateral (spanwise) coordinates
Y_o	lateral location of the fixed hot wire
Z,z',z''	transverse (vertical) coordinates
α_i	empirical constants to fit the autocorrelation function of fluctuating velocities
β	scale of anisotropy of turbulence in the trailing edge wake

δ	thickness of the shear layer in the trailing edge wake
δ_f	flap deflection angle
λ	longitudinal decay rate of correlation function
ω	frequency, radians per second
ϕ	microphone plane - plane passing through jet axis ($\phi = 0^\circ$ corresponds to the plane parallel to the wing surface)
ψ	angle from the trailing edge flow direction
ρ	density of air
τ	time delay between the two hot wire signals
θ	angle between the forward jet axis and the microphone
θ_N	nozzle impingement angle
θ''	angle between the forward direction of flap trailing edge and the microphone (figure 12)

FLOW CHARACTERISTICS

USB flow characteristics were evaluated to insure good flow spreading and turning on the flaps for the acoustic test configurations and as an aid to better understand the noise generating mechanisms. These studies consisted of flow visualizations and flow measurements. Flow visualization tests were run at the highest jet nozzle pressure ratio (1.55) that was used in the acoustic tests. Flow measurements, with hot wire apparatus, were obtained with a low nozzle pressure ratio (1.1) in order to prevent excessive hot wire breakage.

Flow Visualizations

Qualitative flow characteristics were observed and interpreted primarily with the use of oil flow patterns on the wing and flap surface, and schlieren pictures of the flow field.

Oil flow patterns. - The effect of various geometric parameters on flow attachment to the surface and turning characteristics were determined qualitatively by surface oil flow pictures. Figure 3 shows typical effects of nozzle impingement angle on flow attachment for a rectangular nozzle. The flow pattern on the wing and flap surfaces is illustrated in these photographs for nozzle impingement angles of 0°, 10°, and 20°. At 0° the flow separated from the surface before reaching the trailing edge. For the case of impingement angles of 10° and higher, the flow attached to the surface and turned along the surface. It may also be observed that the flow spreading on the surface increases as the impingement angle increases. The other parameters that were varied to study flow attachment effects were: Nozzle shape (rectangular, AR = 8, 4, 2; circular; D-shaped; and elliptical), nozzle chordwise location ($X_N/_C = 0.2, 0.5$), flap knee radius of curvature ($R_C = 5.08$ cm, 7.62 cm), and flap trailing edge length ($L_{TE} = 3.81$ cm and 6.47 cm).

Flow spreading and turning along the surface are related to the "scrubbed area." Since it was not practical to measure the actual scrubbed area on the surface, it was calculated empirically from measurements of the widths in photographs at several chordwise locations. The effects of various geometric parameters on the scrubbed area, are shown in figure 4. The observations made from these experiments are summarized in Table 1. For $\theta_N > 10°$ and $X_N/_C = 0.2$, the flow is fully attached to the wing and flap surfaces. As the nozzle moved towards the trailing edge, however, the nozzle impingement angle has to be increased to obtain the attached flow. It was observed that $\theta_N = 20°$ and $X_N/_C = 0.2$ are good nozzle conditions to obtain attached flow with good flow turning capability.

Schlieren photographs. - The schlieren technique was used to study the flow structure over the wing and flap surfaces and in the trailing edge wake.

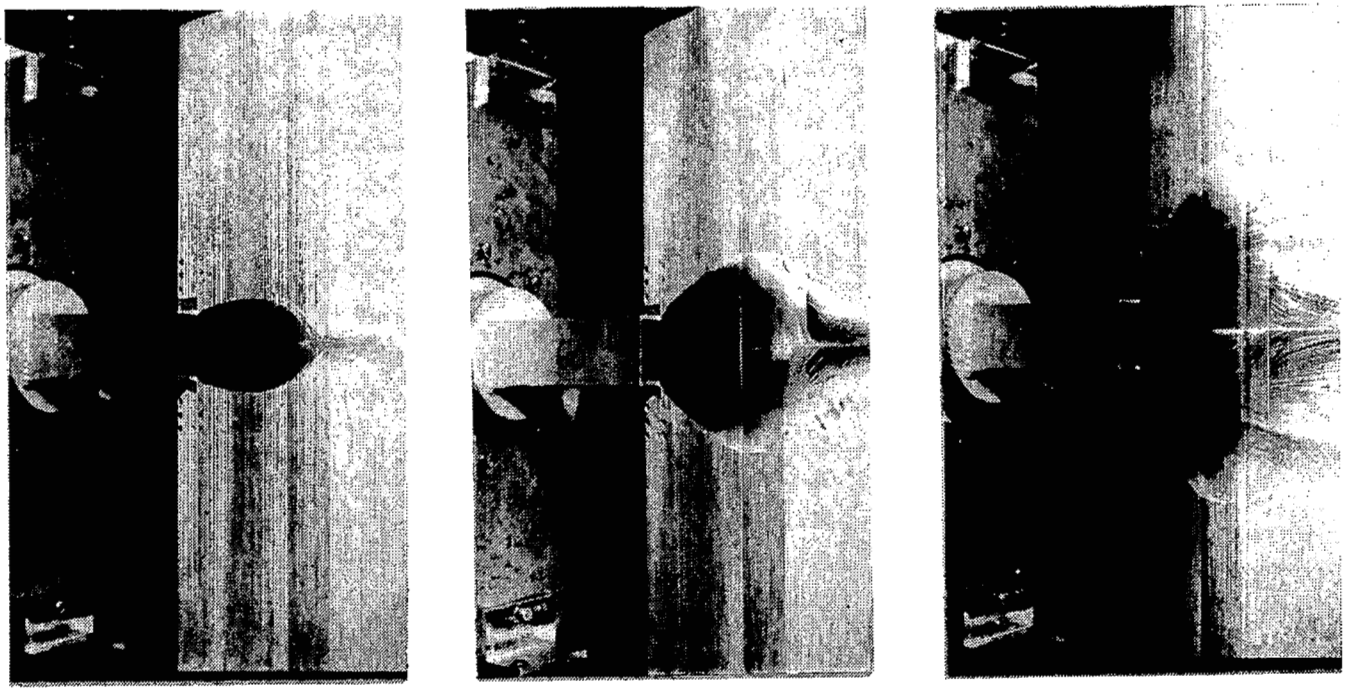

$\theta_N = 0°$ $\theta_N = 10°$ $\theta_N = 20°$

Figure 3. Effect of Impingement Angle - Oil Flow Photographs

AR-2 NOZZLE, $A_N = 20.25\ cm^2$ $\frac{X_N}{C} = 0.2$

$R_C = 5.08$ cm
$\delta_f = 60°$
$L_{TE} = 6.47$ cm

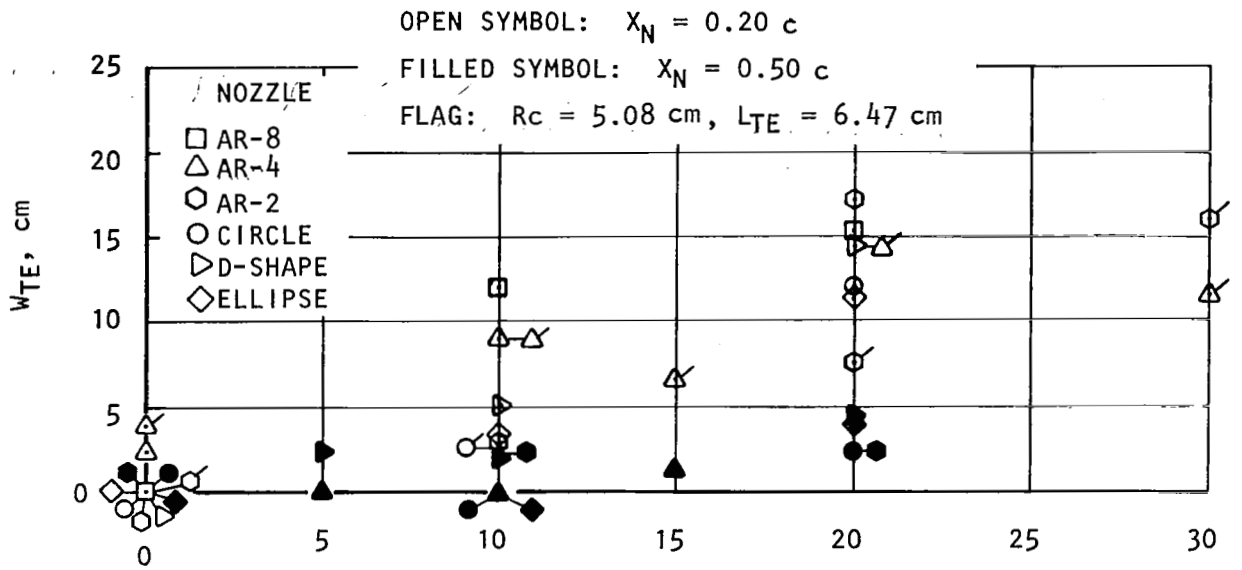

(A) SCRUBBED WIDTH.

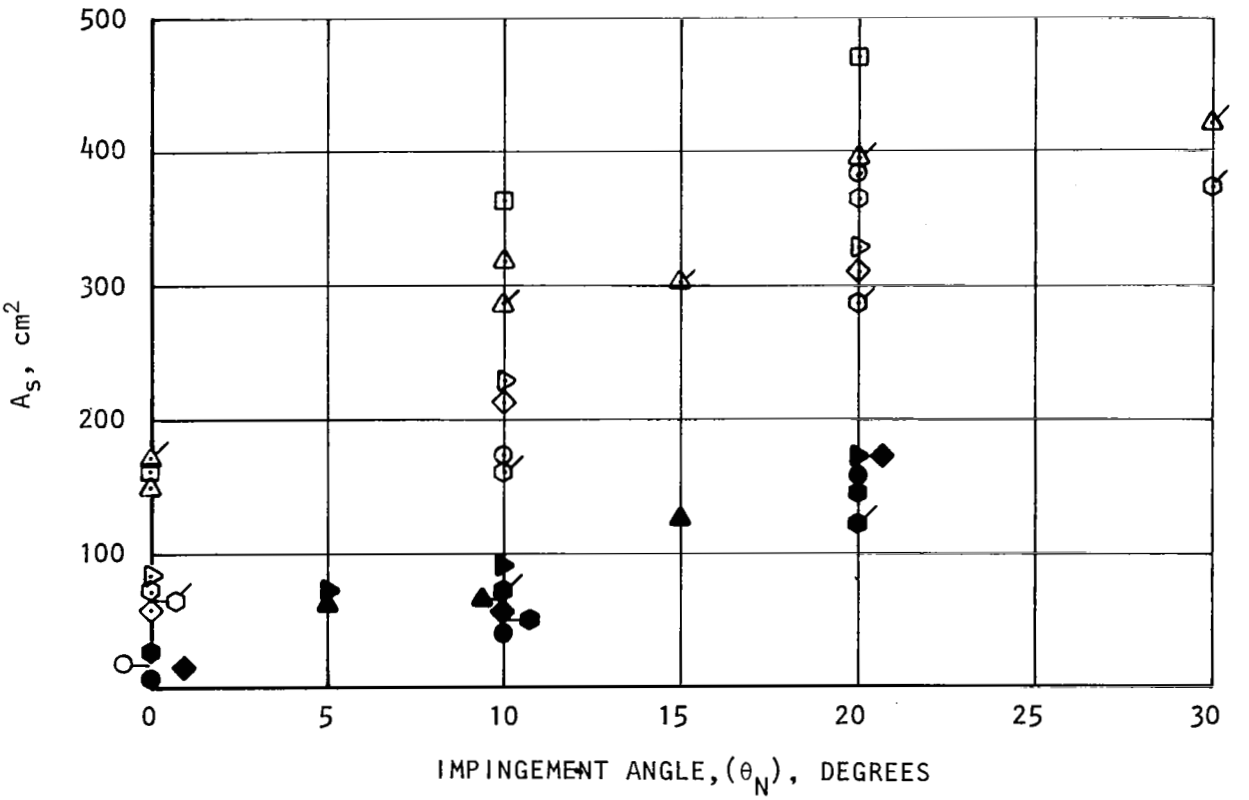

(B) SCRUBBED AREA

Figure 4. Configuration Effects on Flow Spreading.
δ_f=60°; R_c=7.62 cm; L_{TE}=3.81 cm; NPR = 1.55.

A. NOZZLE EFFECTS — LARGE RADIUS FLAP

θ_N(deg) \ $\frac{X_N}{c}$	0.2		0.5	
	SEPARATED	ATTACHED	SEPARATED	ATTACHED
0	AR-8, AR-2, Circle D, Ellipse	AR-4*, QCSEE*	AR-2, Circle, QCSEE	
2			Ellipse	
5				D
10		AR-8, AR-4, Circle, QCSEE, D, Ellipse	Circle, Ellipse	AR-2*, QCSEE*, D
15				
20		AR-8, AR-2, Circle, Ellipse, D		AR-2, Circle QCSEE, D, Ellipse
	$R_c = 7.62$ cm, $L_{TE} = 3.81$ cm, NPR = 1.55			

B. NOZZLE EFFECTS — SHORT RADIUS FLAP

θ_N(deg) \ $\frac{X_N}{c}$	0.2		0.5	
	SEPARATED	ATTACHED	SEPARATED	ATTACHED
0	AR-4*, AR-2			
10		AR-4, AR-2		AR-2
15		AR-4		
20		AR-4, AR-2		AR-2
30		AR-4		
	$R_c = 5.08$ cm, $L_{TE} = 6.47$ cm, NPR = 1.55			

C. NPR EFFECTS vs θ_N

NPR \ $\frac{X_N}{c}$	20%		50%	
	SEPARATED	ATTACHED	SEPARATED	ATTACHED
1.1			$\theta_N = 0°$, 5°, 10°	$\theta_N = 15°$, 30°
1.3		$\theta_N = 0°$		
1.35		$\theta_N = 0°$		$\theta_N = 0°$, 10°, 20°
1.45		$\theta_N = 0°$		$\theta_N = 0°$, 10°, 20°, 30°
1.55				
	AR-4, $R_c = 7.62$ cm, $L_{TE} = 3.81$ cm			

* INDICATES UNCERTAINTY

Table 1. Flow Attachment Observations Using Oil Flow ($\delta_f = 60°$)

Typical schlieren photographs taken in the spanwise direction for different nozzle impingement angles are shown in figure 5. The following observations were made from this study.

- The thickness of the flow field increased with flap deflection, decreased with nozzle impingement angle, and appeared to be relatively independent of flap radius of curvature.

- The spreading angle below the wing/flap in the trailing edge wake was fairly insensitive to both flap radius of curvature and flap deflection angle.

- From these results, the reference test configuration was selected to be the AR = 4 rectangular nozzle with pitch angle $\theta_N = 20°$ and located on the wing at $X_N/_c = 0.2$. This configuration was used to evaluate the basic noise characteristics and the effect of geometric parameters on noise were studied by varying the parameters about this configuration.

Flow Measurements

Profiles. - Mean velocity and turbulence intensity profiles were measured, using hot wire techniques, at various longitudinal and lateral (spanwise) locations in the trailing edge wake. Typical mean velocity and turbulence intensity profiles just downstream of the trailing edge are shown in figures 6 and 7, which illustrate that the velocity gradient and the turbulence intensity are very large close to the surface (small z'). The following observations were made from this phase of study.

- Increased nozzle areas tend to have higher peak velocities and have peaks located near the surface.

- As the spanwise distance from the jet centerline increased, the magnitude of the velocity peak reduced and thus the velocity gradient was also reduced.

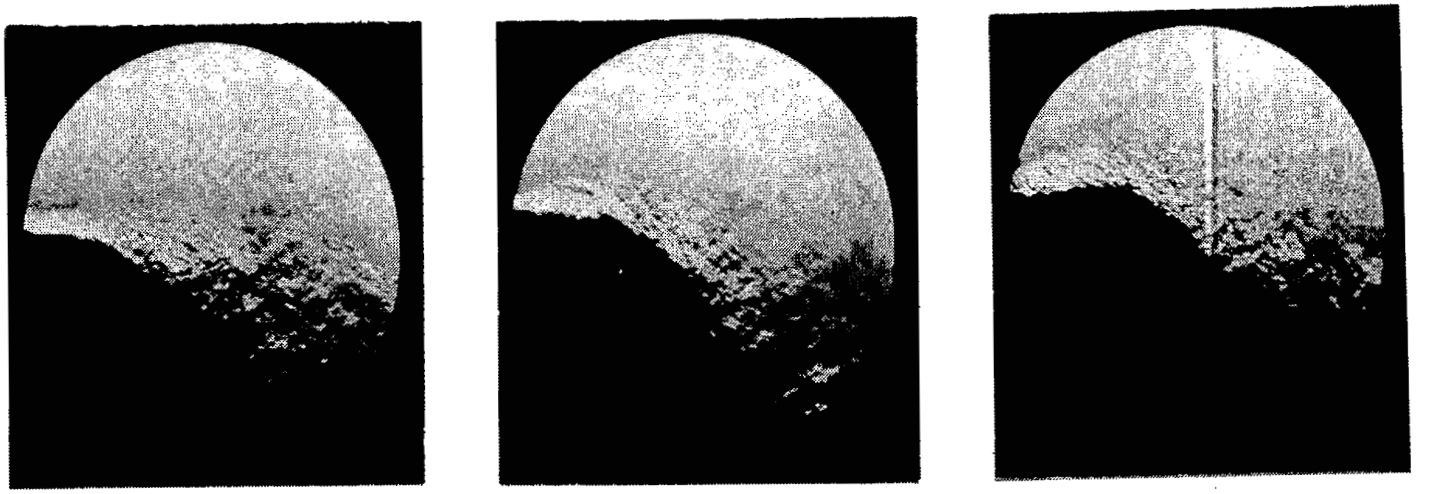

$\theta_N = 0°$ $\theta_N = 10°$ $\theta_N = 20°$

Figure 5. Effect of Impingement Angle - Schlieren Photographs

AR-8 NOZZLE
$X_N/c = 0.2$
$R_c = 7.62$ cm
$\delta_f = 60°$
$L_{TE} = 6.47$ cm

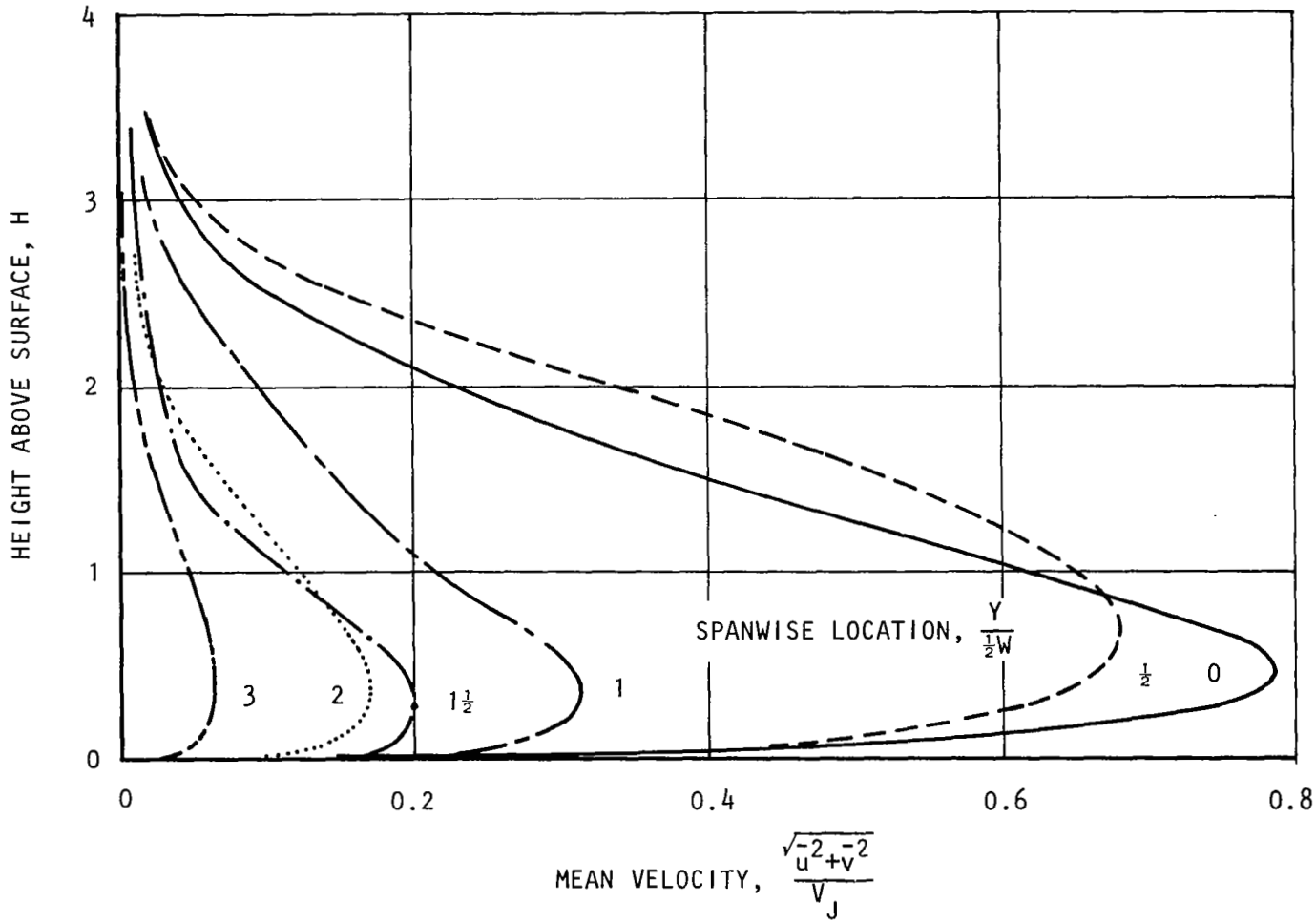

Figure 6. Mean Velocity Profiles - Just Downstream of Trailing Edge

AR-4 NOZZLE θ_N = 20° δ_f = 60°
X_N/c = 0.2 R_c = 5.08 cm L_{TE} = 3.81 cm

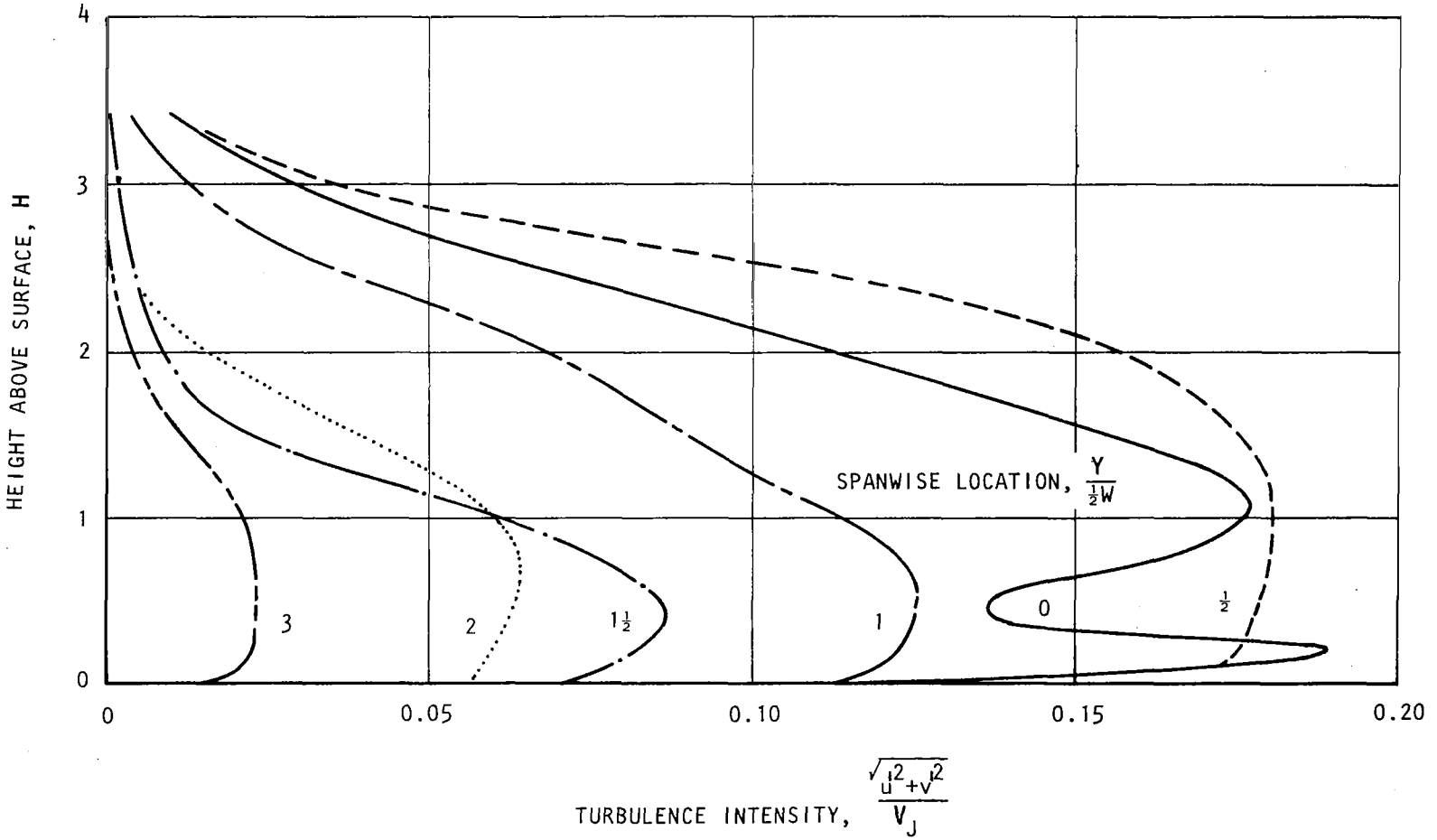

Figure 7. Turbulence Intensity Profiles - Just Downstream of Trailing Edge

AR-4 NOZZLE $\theta_N = 20°$ $\delta_f = 60°$
$X_N/c = 0.2$ $R_c = 5.08$ cm $L_{TE} = 3.81$ cm

- As the nozzle moved towards the trailing edge, the mean velocity increased and the peak velocity peak moved closer to the surface. Better turning was achieved when a straight section followed the curved section rather than preceded it. This improved turning is due to the longer trailing edge allowing smoother adjustment from the coanda-reduced pressure on the curved surface towards the trailing edge section.

- Increasing the trailing edge length reduced the peak velocity and the turbulence intensity.

- Decreasing the flap radius of curvature reduced the peak velocity and increased the peak turbulence intensity.

- Freestream flow (forward speed effects) promoted lateral spreading of the jet.

- Smaller flap deflection angles promoted attachment and turning and tend to decrease the turbulence intensity in the outer mixing region.

These results indicated that the mean velocity profiles just downstream of the trailing edge had broad maxima, reflecting the fact that the flow was similar to that of a free jet (without wing and flap). Also, a large velocity gradient close to the surface was evident. The turbulence level was quite large over a substantial portion of the wake thickness. Since the velocity gradient was small away from the shear layer, turbulence was not generated there, but instead, was generated upstream and convected by the mean flow. But in the shear layer, close to the flap surface, intense turbulence was generated which can be associated with the large velocity gradients.

Space-time correlation of turbulence. - The region of high turbulence at the trailing edge was thought to be a region of intense noise generation. Therefore, the characteristics of the fluctuating velocities were evaluated in this region using space-time correlations. These data were used primarily

in conjunction with the theoretical acoustics development discussed in a later section.

Space-time correlations of the fluctuating velocities in the streamwise, lateral (spanwise), and transverse (vertical) directions were measured. A typical space-time correlation function in the streamwise direction for various separation distances is shown in figure 8. The turbulence parameters such as decay rate, length and time scales of the turbulence structure were derived from these correlation functions. The length scales in the longitudinal and lateral directions were found to be 0.84 and 0.366 cm, respectively. The ratio of these two length scales (2.3) is defined as the scale of anisotropy. This value is comparable to that measured in the initial mixing layer of turbulent jets. The convection velocity of turbulence is found to be 0.9 times the peak mean velocity in the trailing edge wake, which is slightly higher than typical values measured in jets. However, considering the difference in the mean velocity profiles between the jet flow and the trailing edge wake flow, this value may not be unreasonable. The longitudinal decay rate of the turbulence (rate of losing coherence of the turbulence) was found to be $2.848/\delta$, where δ is the characteristic thickness of the shear layer in centimeters. The power spectra of turbulence pressure was modeled by assuming it has a similar form as that of surface fluctuating pressures in boundary layer flow.

ACOUSTIC CHARACTERISTICS

Experimental investigations were conducted to evaluate the USB noise characteristics of the following:

1. Parametric Effects - Effects of various geometric and operational variables.

2. Scale Effects - Effect of the geometric size.

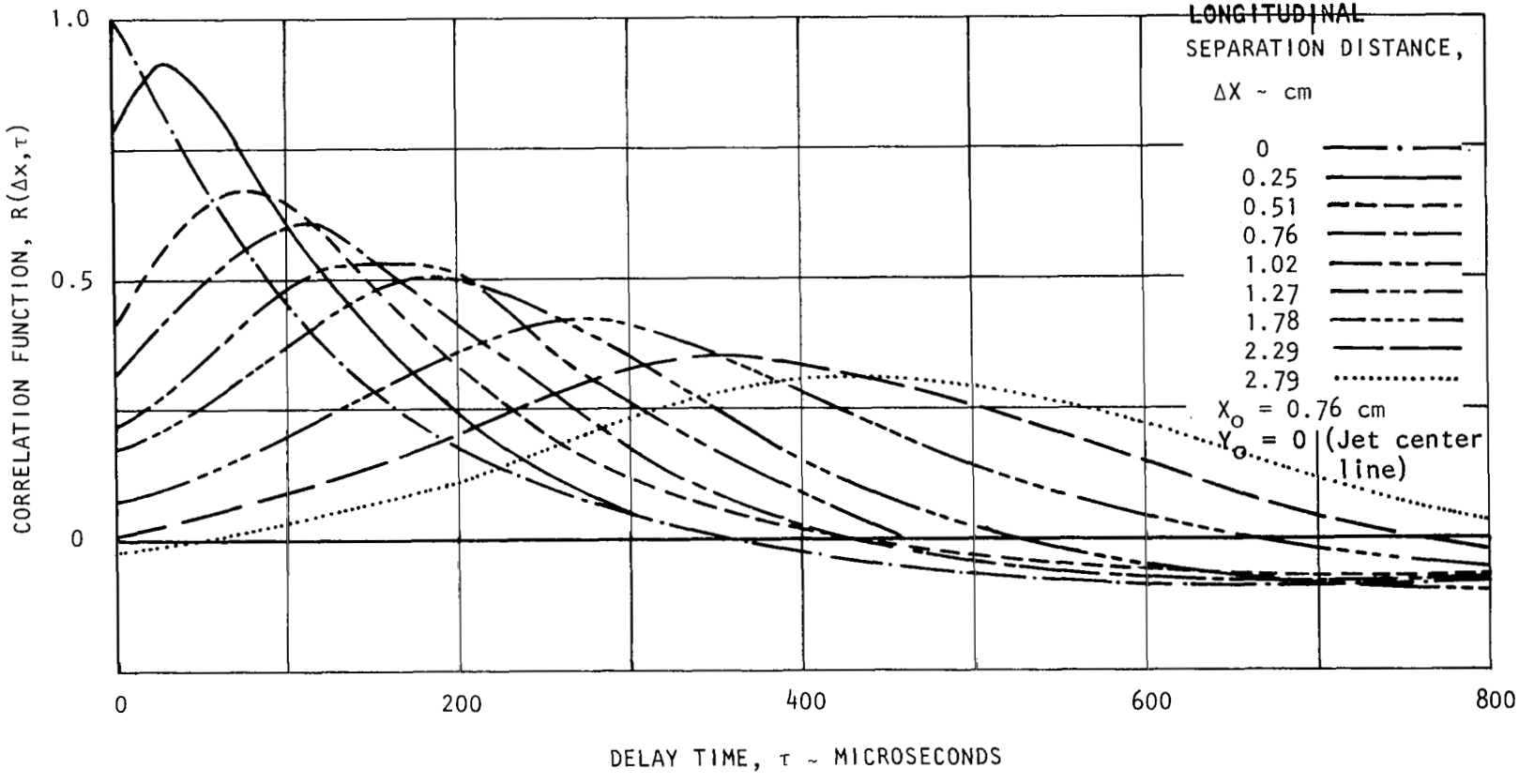

Figure 8. Streamwise Correlation of Turbulence in the Trailing Edge Wake

AR-8 NOZZLE $\theta_N = 20°$ $R_c = 7.62$ cm $L_{TE} = 6.47$ cm
$X_N/c = 0.2$ NPR $= 1.1$ $\delta_f = 60°$

3. Forward Speed Effects - Effect of simulated aircraft motion.

4. Noise Reduction Concepts - Feasibility of noise reduction through various passive and active concepts.

The information obtained from these tests comprise the major part of the experimental data base program. Due to the several test facilities used, and numerous individual test configurations and test points, only some of the more significant trends and characteristics are discussed here. Reference 1 contains the detailed catalog of noise data from which the following paragraphs are derived.

Parametric Effects

Experiments were conducted in an anechoic chamber using a small USB model under static conditions to evaluate the sound pressure levels, directivity and spectral distribution of far-field noise. Geometric and operational parameters were varied systematically in order to study the effect of each. The following are the parameters and their ranges used in this part of the investigation:

Nozzle Area and Shape –	20.26 cm^2 - circular, rectangular with aspect ratio of 8 and 4; 10.13 cm^2 - circular, D, ellipse, rectangular with aspect ratio 2; 21.6 cm^2 - modified D, fixed version of a simulated variable geometry nozzle (QCSEE).
Nozzle Impingement Angle –	0°, 10°, 15°, 20°, 30°, 40°.
Nozzle Longitudinal and Vertical Position –	X/c = 20%, 35%, 50% z = 0, 1.27 cm, 1.59 cm, 2.54 cm.

Flap Length – 8.4 cm to 18.4 cm.

Flap Radius of Curvature – 5.08, 7.62 and 10.16 cm.

Flap Angle – 0°, 30°, 45°, 60°.

Nozzle shape. - As the aspect ratio of the nozzle increased, the noise levels decreased – particularly in the mid-frequency range. The general indication is that a decrease in spanwise jet spreading on the wing/flap surface resulted in an increase in noise level. In the case of the variable geometry nozzle, however, the noise levels increased mainly in the high frequency range, probably because of noise generated by the nozzle side door openings.

Nozzle area. The effect of nozzle area was investigated with the basic circular nozzle shape by varying the diameter, while holding the wing and flap geometry fixed. Not surprisingly it was found that the noise increased with an increase in nozzle area. An increase in nozzle area alone, however, does not change the spectral shape of the radiated sound.

Nozzle impingement angle. - As the nozzle impingement angle increased, the noise levels tended to decrease slightly in the mid-frequency range. If the flow separated from the surface ahead of the trailing edge, as in the case of 0° impingement angle, then the noise level dropped markedly. Therefore, the increase in impingement angle has essentially the same effect as that of an increase in aspect ratio of the nozzle. In both bases (with attached flow), the flow spread spanwise over the wing and flap surfaces and probably reduced the flow velocity at the trailing edge. It should be noted that an increase in nozzle impingement angle reduced the effective nozzle area which caused a lower mass flow for a given velocity, and consequently lower thrust. When the noise is corrected for this change in thrust, the noise levels correlate better, but there is still a consistent moderate reduction in the middle frequencies with increasing impingement angle.

Nozzle longitudinal position. - As the nozzle was moved from 0.2 c to 0.5 c towards the trailing edge, the magnitude of the noise levels did not increase significantly, but the spectrum appears to shift towards higher frequencies. It should be noted, however, that this is true only for the cases with attached flow.

Nozzle vertical position. - The effect of nozzle vertical position on the noise characteristics is not simple to analyze. This parameter has to be combined with the nozzle pitch angle and probably with the nozzle longitudinal location to achieve the required flow spreading and turning. In this program, systematic parametric studies were not conducted to evaluate the noise for the same or similar performance. However, preliminary experimental results indicate that the noise levels in the low frequency range were reduced as the nozzle moved away from the wing. No consistent trends were observed in the velocity exponents and directivities.

Flap length. - As the trailing edge section of the flap was increased in length, the spectrum shifted to lower frequencies, but the magnitude of the noise was not changed. The variation in spectra was very similar to that of a change in nozzle longitudinal location.

Flap radius of curvature. The radius of curvature of the flap was varied, keeping the total flow length constant. The flap angle was also kept constant by changing the lengths of curved and straight portions of the flap. In addition, the radiated sound was also measured with zero flap angle (where the curved section of the flap was replaced by a straight section). These results indicated that the effect of radius of curvature on far-field sound was negligible, provided that the flow was attached on the wing and flap surfaces.

Flow path length correlations. - Following the discussion of effects of nozzle longitudinal position, flap length, and flap radius of curvature, it is concluded that the flow length (defined as the length on the surface from the nozzle exit to the flap trailing edge) is a significant parameter which can be varied by changing either the nozzle longitudinal position or the flap

length. A nondimensional frequency (Strouhal number) for USB noise was developed with this parameter and is defined as $S = fL_F/V_J$, where f = center frequency of noise one-third octave bands, L_F = flow length, and V_J = jet exit velocity. Typical resulting nondimensionalized spectra, given in figure 9, show that the data correlate very well. Since the flow path length and jet exit velocity are readily available quantities, they are very useful parameters for defining Strouhal number in USB noise predictions.

Flap angle. - The effect of flap angle on the radiated sound field was primarily a shift in directivity. The experimental results indicate that the sound field tends to rotate with changes in flap angle. Figure 10 shows normalized data for three flap angles in the flyover plane at a constant angle relative to the flap upper surface. The flap deflection angle is included in the nondimensional parameter illustrating the method devised to account for flap angle effects.

Jet exit velocity. - The jet exit velocity is obviously an important parameter affecting far-field noise. The magnitude of the radiated sound field varied as jet exit velocity raised to a power between 5.5 to 7.8 depending on the angle of propagation. The variation of the spectral distribution with jet velocity is shown in figure 11 and the variation of the velocity exponent with the direction is illustrated in figure 12.

Jet exit temperature. - The effect of jet temperature on USB noise was investigated using a jet flow with one elevated temperature (93°C) in addition to the usual ambient jet temperature (approximately 26°C). These preliminary results indicated that the noise levels in the high frequency range were reduced as the jet flow temperature increased. Since the temperature experiments were limited, these results cannot be generalized.

Scaling Effects

The scale effects of the USB configuration on far-field noise were investigated using two geometrically similar configurations of two sizes (one in the anechoic room and the other at the acoustic and performance facility).

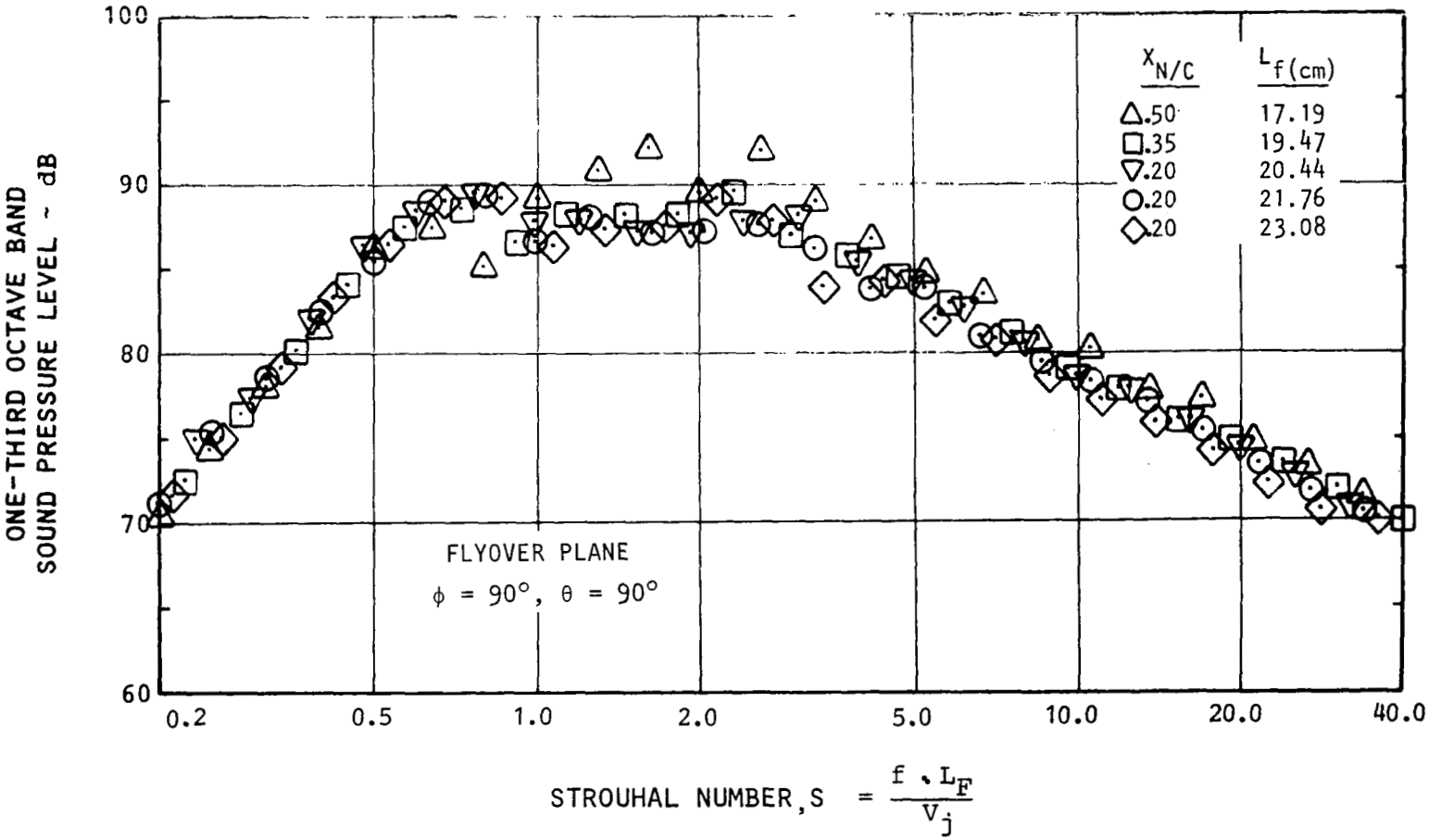

Figure 9. Correlation of Nondimensional Frequency Based on Flow Length

AR-4 Nozzle, V_J = 215 m/sec
$\delta_f = 30°$, R_c = 7.62 cm

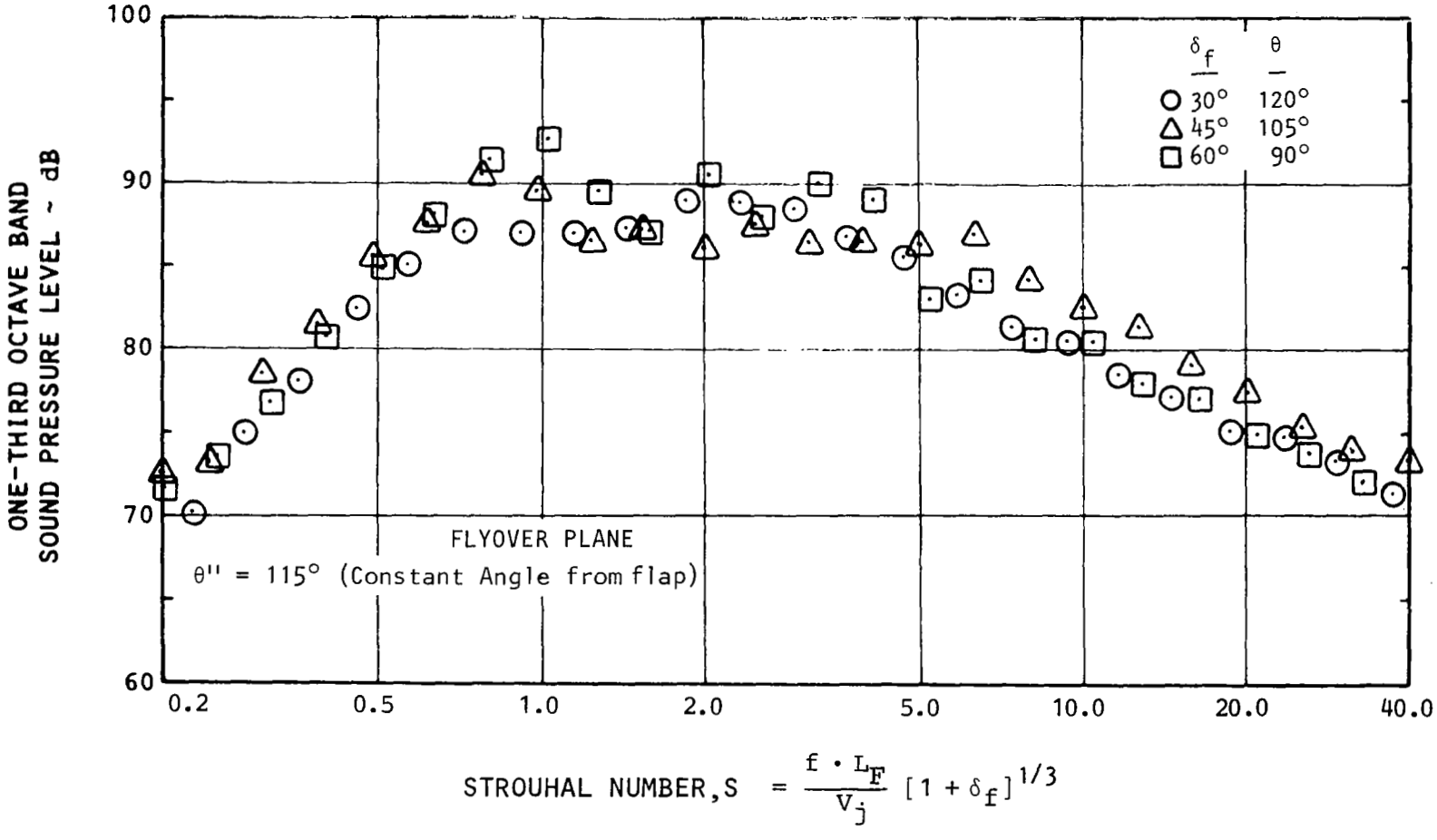

Figure 10. Effect of Flap Angle on Non-Dimensionalized Spectrum

AR-4 NOZZLE R_c = 7.62 cm
L_f = 21.76 cm V_J = 180 m/sec

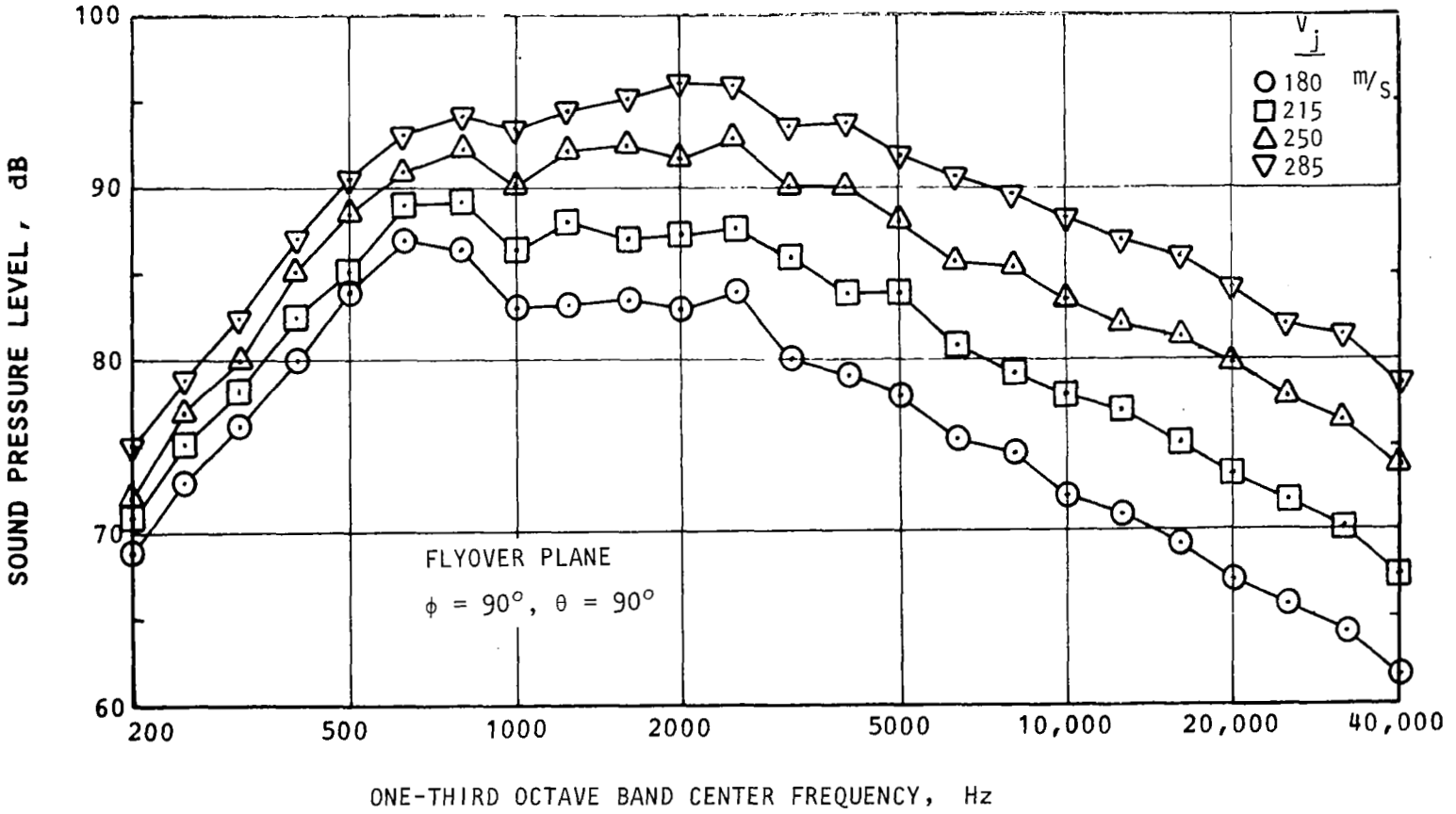

Figure 11. Effect of Jet Velocity on Spectrum

AR-4 NOZZLE $X_N/c = 0.2$ $\delta_f = 30°$
$\theta_N = 20°$ $R_c = 7.62$ cm

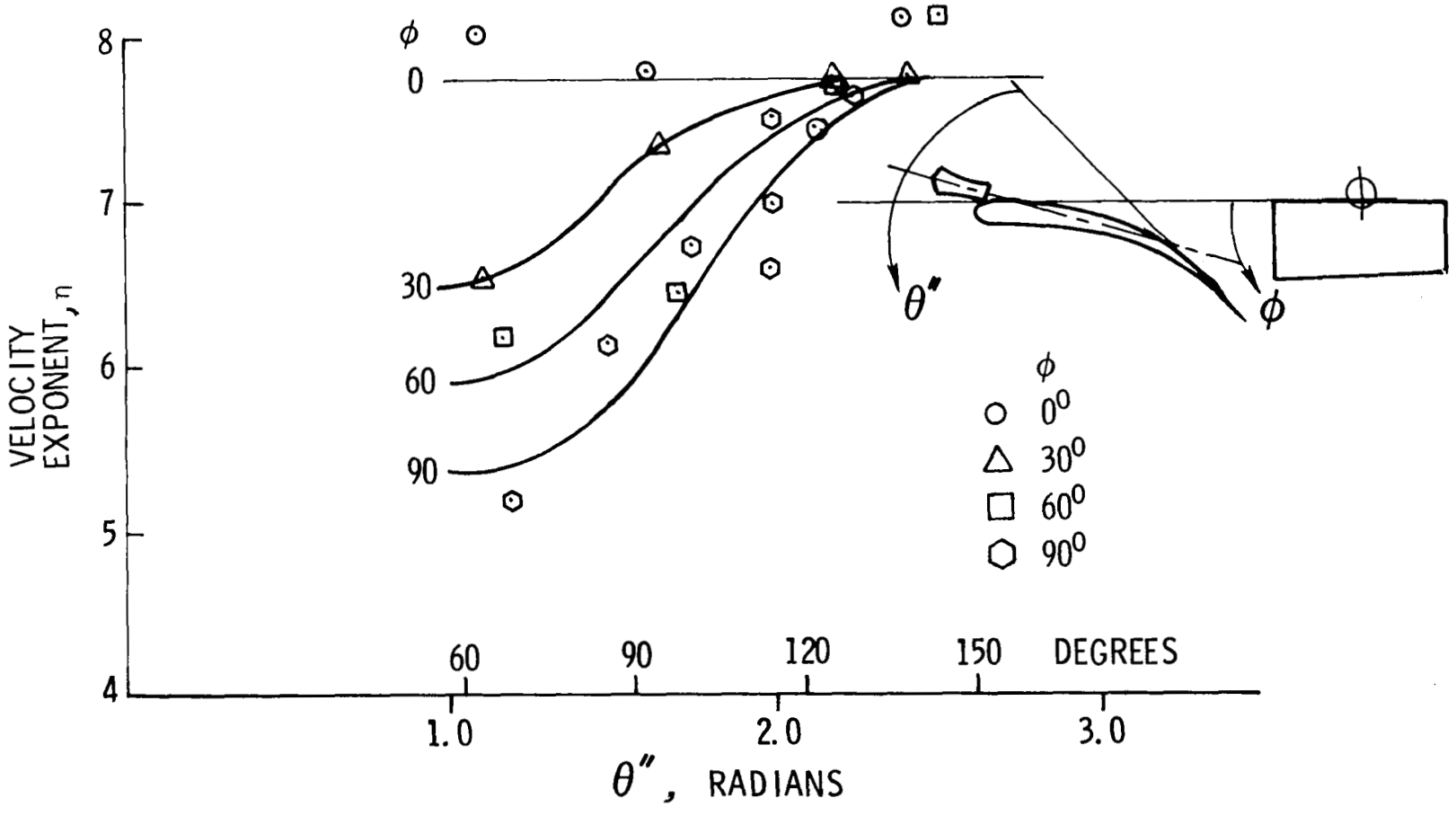

Figure 12. Velocity Exponent vs. Directivity Angles θ'' and ϕ

The linear scale ratio between the two models is 2.37. The sound pressure level spectral comparisons in the flyover plane are shown in figure 13. The microphone distances from the jet exit center were 2.4 m and 6.1 m for the small- and large-model tests, respectively. The noise data from the small model were scaled to the large model by assuming the sound pressures were directly proportional to the area of the nozzle and inversely proportional to the square of microphone distance, and that the frequencies were inversely proportional to the model linear scale. Thus, the small model data were corrected by increasing the SPL's by (20 log 2.37 + 20 log 2.4/6.1) and shifting down the frequencies by 1/2.37. In addition, atmospheric attenuation was corrected to the appropriate distances and frequencies. The good agreement between the data for the two sizes in this figure confirms that linear scaling is adequate for geometrically similar models.

Forward Speed Effects

Limited investigations were conducted to study the effect of aircraft flight on noise. These experiments were conducted in the Lockheed anechoic free-jet facility which is an open throat wind tunnel with an anechoic test section.

Low frequency noise was generally reduced with an increase in free-stream velocity as shown in figure 14. The high-frequency noise was reduced by a small amount in the forward quadrant. In the aft quadrant, however, the noise levels in the high frequency range increased with an increase in free-jet stream velocity (simulated aircraft motion). This is illustrated in figure 15. This is probably due to a shift in directivity. In order to fully understand the noise characteristics of USB with forward speed, additional acoustic and flow investigations must be conducted.

Noise Reduction Techniques

Since the dominant USB noise generating mechanism is in the vicinity of the trailing edge, it was desirable to modify the flow characteristics or the acoustic impedance of the surface near the trailing edge to reduce the radiated

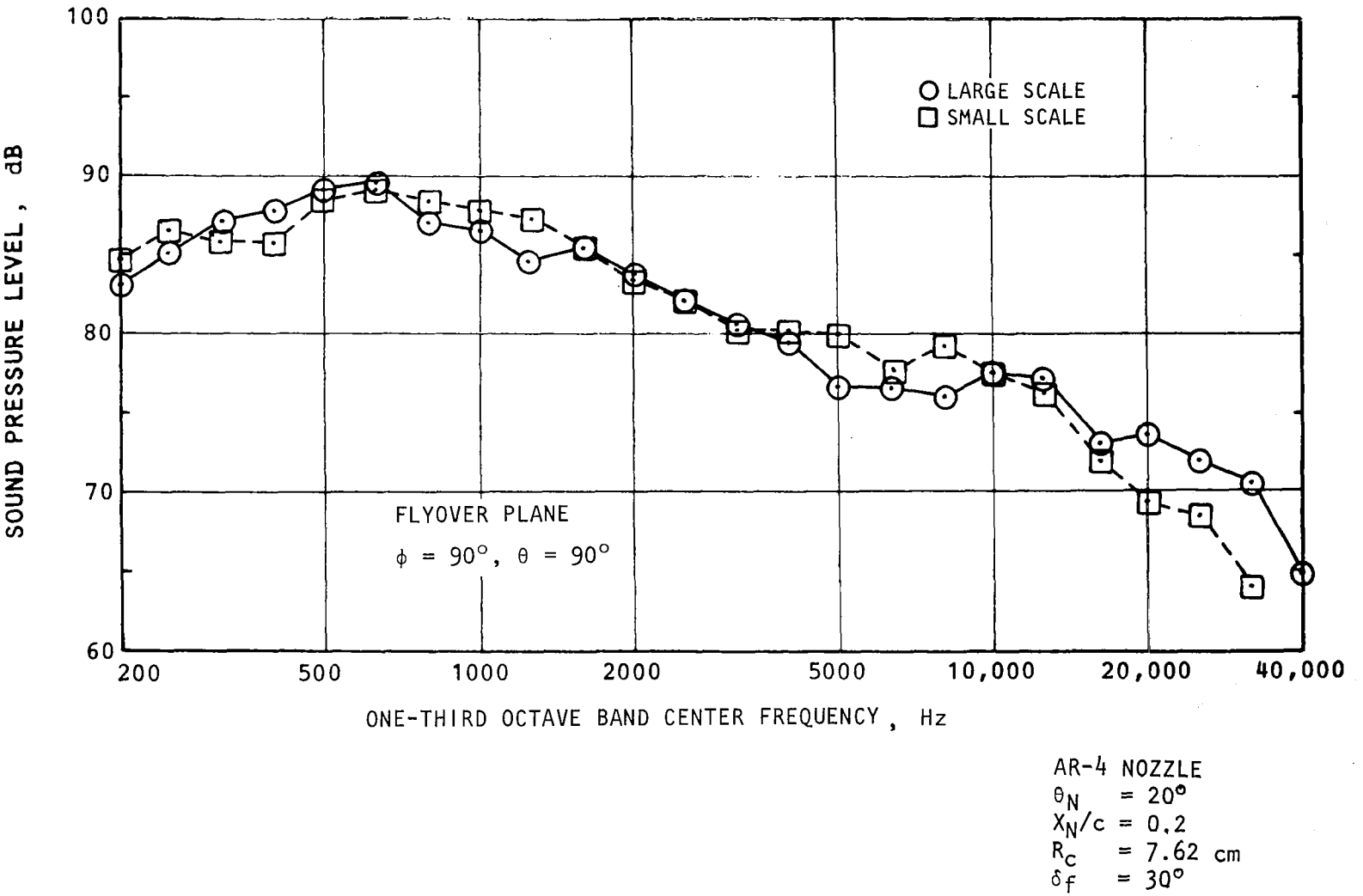

Figure 13. Effect of Model Scale on Spectrum
(Data corrected to large model size.)

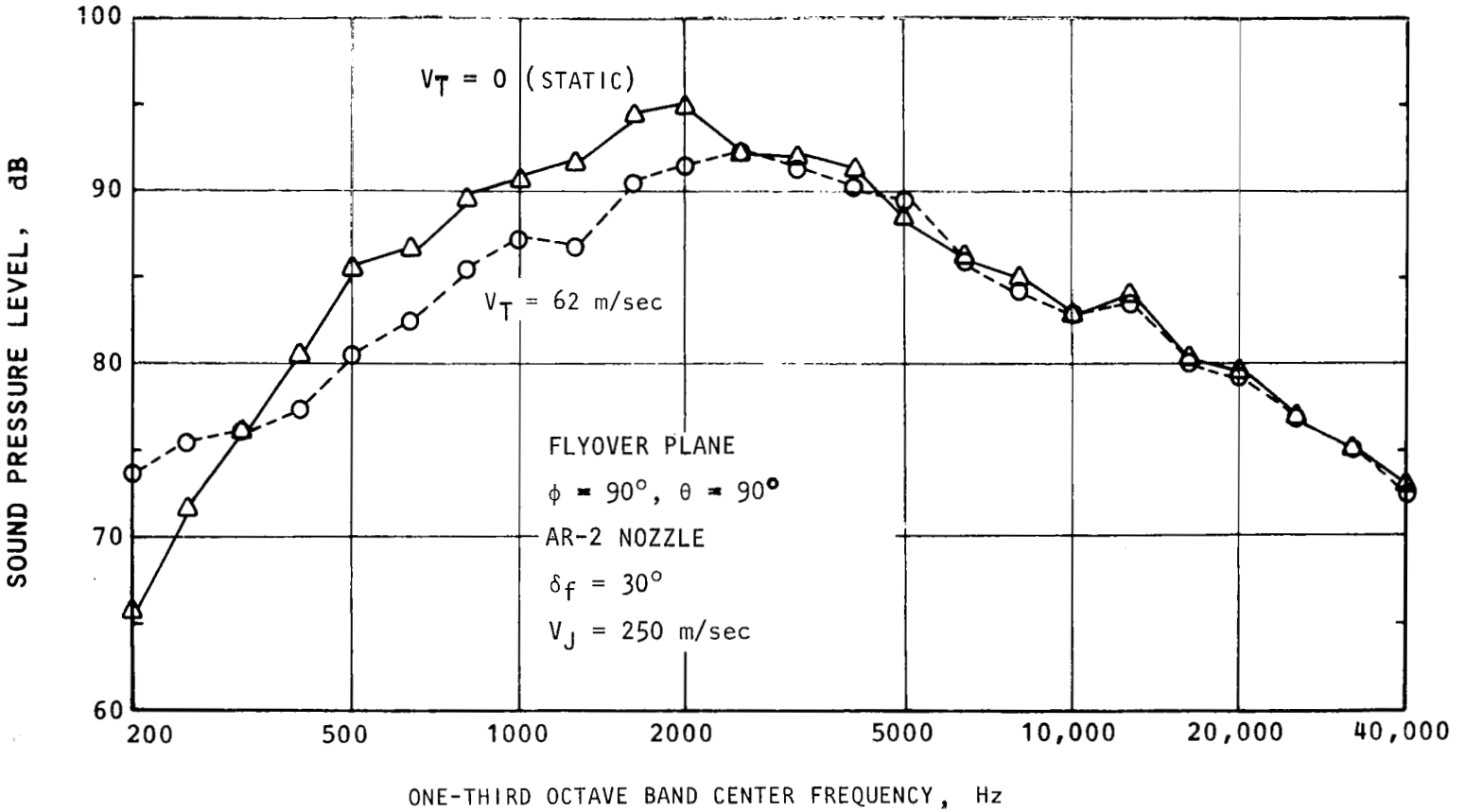

Figure 14. Effect of Forward Speed on Spectrum

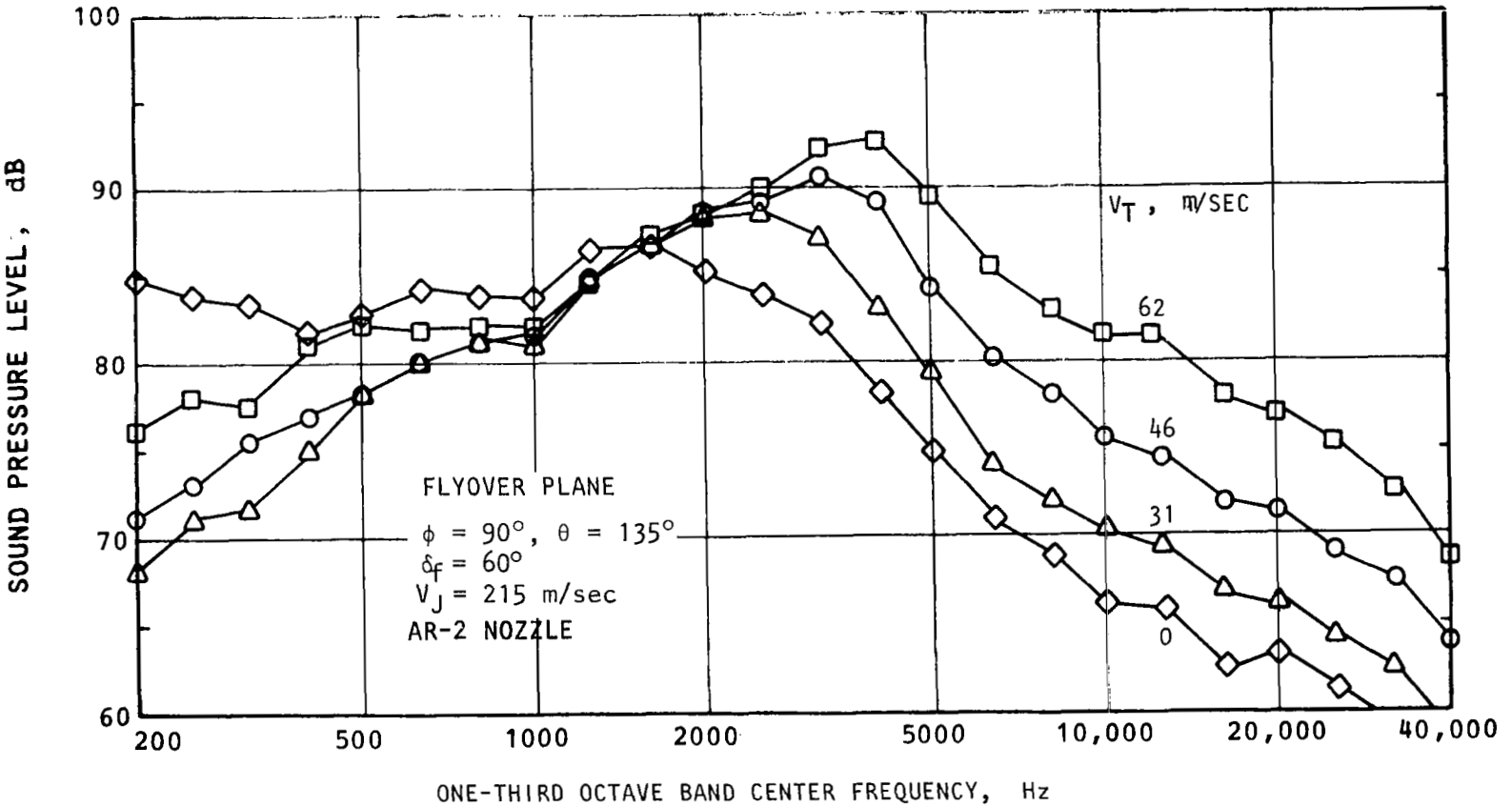

Figure 15. Example of Increase in High Frequency Noise in the Aft Quadrant with Increasing Forward Speed

sound field. Therefore, the following techniques were investigated experimentally: (1) replacement of the flap upper surface with acoustic materials or extending the flap with porous material, (2) secondary air blowing through a slot close to the trailing edge, and (3) use of streamwise splitters at the flap trailing edge. These tests were rather complex and details are given in references 1 and 2. However, some generalized highlights are given in the following paragraphs.

The configurations with a complete upper surface acoustic treatment showed a small reduction in flyover noise and a small increase in sideline noise. The configurations with half of the surface treated indicated an increase in both flyover and sideline noise. However, configurations with porous trailing edge extensions produced a reduction in both flyover and sideline noise. The combination of complete treated upper surface and porous trailing edge extension produced a substantial reduction in flyover noise, but very little change in sideline noise. The configuration with streamwise trailing edge splitters had a very small reduction. Attempts were not made to optimize either the impedance of treatment or the spacing of the splitters.

Introduction of secondary blowing near the trailing edge (just ahead of the edge on the upper surface) had a significant effect on noise. Two parameters of slot blowing, the slot height and the ratio of slot velocity to jet exit velocity were investigated. Typical results are shown in figure 16. The spectral results and the directivity indicate that noise reduction may be obtained at all frequencies and in both forward and aft directions. However, the noise reduction at high frequencies are greater than at low frequencies.

Comparison With Other Data

Measured noise data were compared with published experimental data reported in references 3, 4, and 5. A typical comparison is shown in figure 17. The levels in this figure are normalized to a nozzle area of 114 cm^2, measured at 6.1 m form the nozzle. The comparison is reasonably good considering some differences in configurations, facilities, and instrumentation.

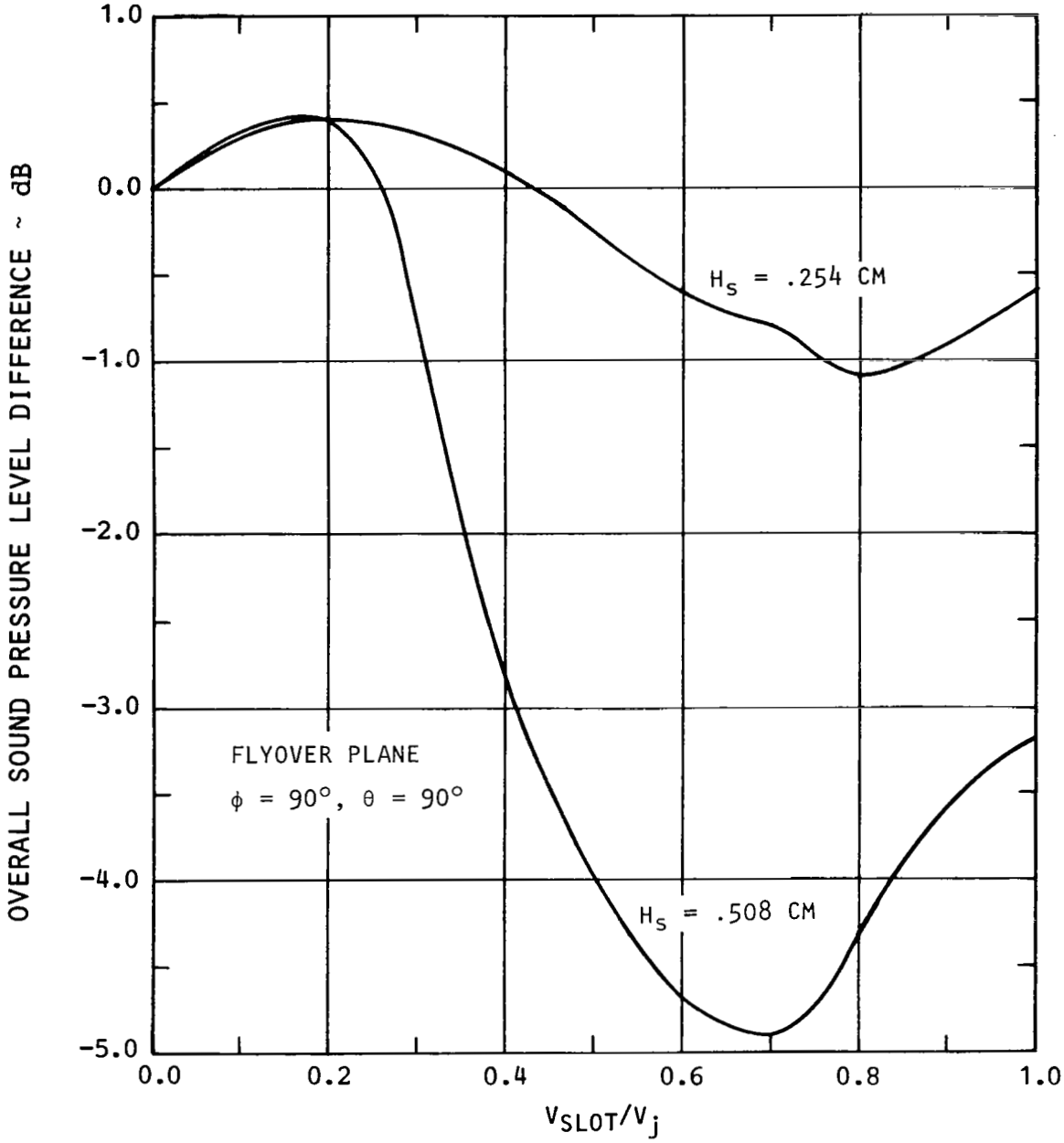

Figure 16. OASPL Reduction Due to Trailing Edge Slot Blowing

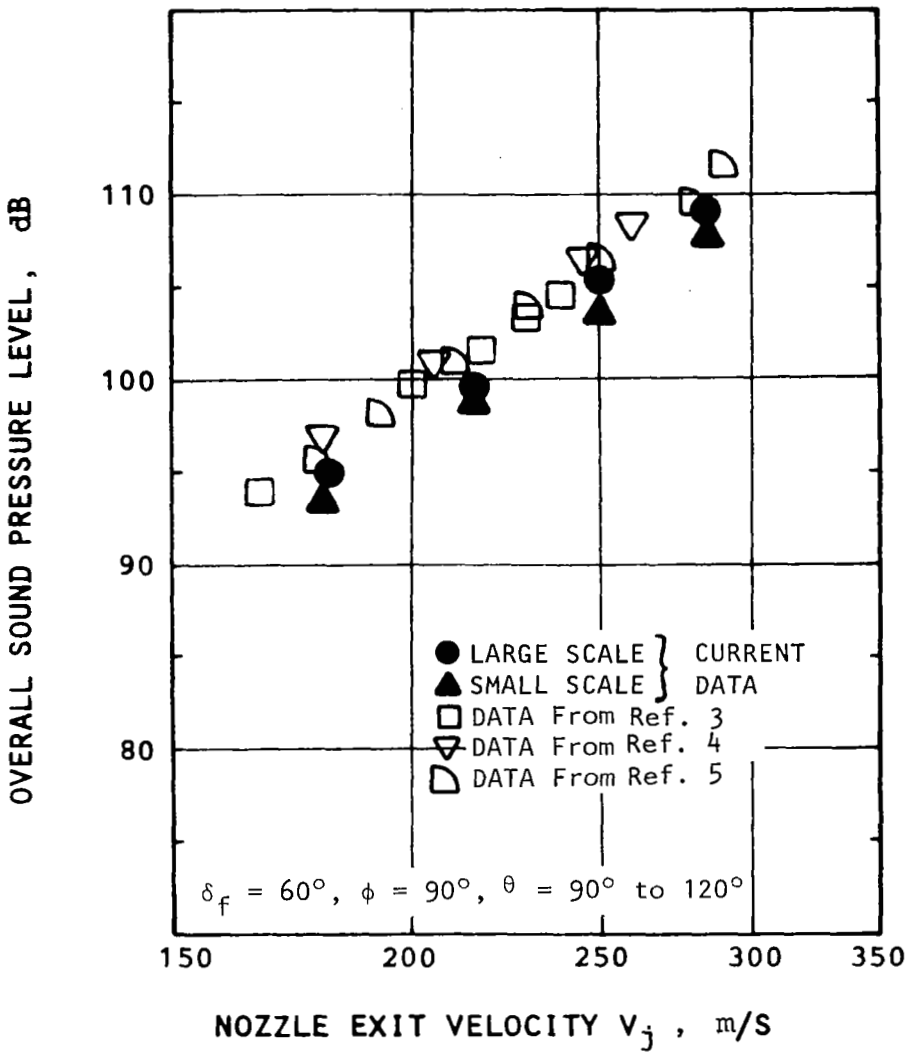

Figure 17. Comparison with Other Data
(Data Scaled to 114 cm^2 Nozzle Area and
6.1 m microphone distance)

Additional Experiments

In addition to the results summarized in this section, the following test results were obtained: (1) Surface fluctuating pressures on the wing and flap surfaces, (2) fluctuating pressures on a simulated fuselage wall close to the flap trailing edge, and (3) correlation between the near-field pressures in the trailing edge wake and far-field (acoustic pressures). These results are presented in reference 1. The fluctuating pressures on the wing and flap indicated that the pressures were maximum at the flap trailing edge on the jet centerline. Fuselage wall pressures indicated that the magnitude increased with jet exit velocity for static cases. With forward speed, however, the pressures were increased slightly for all jet velocities, but the variation with jet velocity was very small. These pressure data indicate that forward speed has a strong influence on the fuselage fluctuating pressures. The correlations of near- and far-field fluctuating pressures indicated that the maximum correlation was obtained for the microphone closest to the trailing edge and decreased progressively downstream.

PREDICTION PROGRAM

The state-of-the-art is not sufficiently advanced to compute USB noise by theory alone. Consequently, noise prediction procedures must be derived by empirical techniques based primarily on an analysis of test data. The data developed under the current program were used in the development of a USB noise prediction program.

As discussed previously, it was found that the flap knee radius of curvature does not have a significant effect on the radiated sound field provided the flow remains attached to the wing and flap surfaces. Flap length and nozzle longitudinal location effects can be combined together as the flow path length effect (length between the nozzle exit and the flap trailing edge on the surface). Far-field noise depends on the flow characteristics at the trailing edge, and the flow velocity and the jet thickness at the trailing edge depend on the flow path length. Thus, it is reasonable to assume that the noise characteristics are functions of flow path length. In fact, the

experimental results did indicate that the flow path length (not nozzle diameter) is the best length scale to be used in the Strouhal number. The sound field directivity changed as the flap angle was changed. However, for a constant angle with respect to the flow direction in the trailing edge wake, the radiated sound field is essentially independent of flap angle. Nozzle exit shape is included as nozzle aspect ratio (ratio of equivalent width to equivalent height) and hydraulic diameter. The magnitude of the radiated sound was found to be directly proportional to the area of the nozzle. The sound pressure is proportional to the jet exit velocity raised to the power n where n varies from 5 to 7.5 depending on the direction. The frequency of the sound pressure is directly proportional to the jet velocity. The following equation is derived for the maximum one-third octave band sound pressure level,

$$\text{Peak SPL} = 10 \log \left(\frac{V_J}{V_o}\right)^n + 10 \log \frac{A_N}{A_o} - 20 \log \frac{R}{R_o}$$

$$- 10 \log \left[(AR_N)^{1/3} \cdot \frac{L_F}{D_H}\right] + K \qquad (1)$$

where V_J - jet exit velocity

A_N - nozzle area

R - distance from the aircraft to the measuring location

AR_N - nozzle aspect ratio

L_F - flow path length

D_H - hydraulic diameter of the nozzle

V_o, R_o, A_o - reference velocity, distance, and area, respectively.

The nondimensional spectral shape is given as

$$\left[\text{SPL} - 10 \log \left(\frac{V_J}{V_o}\right)^n - 10 \log \frac{A_N}{A_o} + 20 \log \frac{R}{R_o}\right.$$

$$\left. - 10 \log \left(AR_N{}^{1/3} \cdot \frac{L_F}{D_H}\right) - K\right] \qquad (2)$$

against modified Strouhal number, $fL_F/V_J\ (1+\delta_f)^{1/3} \cdot F_s$, where δ_f is the flap angle in radians, and n, K, and F_s are functions of directivity, θ and ϕ. The spectral shape is shown in figure 18, and comparisons between the predicted and static measured data show the agreement to be good.

Based on the preceding for blown flap noise, a computer program has been developed to predict the noise of a complete USB aircraft. This program predicts one-third octave spectra, PNL, and OASPL at any given observer location. A footprint program is also available to generate EPNL contours. A simplified flow chart of the complete program is shown in figure 19.

INTEGRATION OF AIRCRAFT NOISE AND PERFORMANCE

A limited USB aircraft design study was performed to determine the compatibility of low noise characteristics with good aircraft performance. This investigation was based on the methods developed to study short-haul transport systems at Lockheed for NASA during 1972-1974. The engines used in this study were those with design fan pressure ratios of 1.35 and 1.47. The salient characteristics of the eight aircraft designs selected for initial screening evaluation are shown in Table 2. Figure 20 shows the 90 EPNdB footprint area for the eight aircraft initially studied. The takeoff noise levels are dictated primarily by the choice of the engine and landing noise as a function of field length.

From the considerations of noise, performance (cruise and low speed), and operating cost, Aircraft 2 with a D-nozzle shape was selected as the baseline design for further study. The effect of various aircraft parameters on performance and noise were investigated. The cruise performance parameters varied were nozzle boattail angle, aspect ratio, relative size and discharge position (derived from companion contract NAS1-13871). Parameters varied to study their effects on noise were nozzle aspect ratio and impingement angle on the wing, flap extension, deflection, and radius of curvature, fan-duct treatment, and USB noise suppression devices. The effect of each of these parameters on the 90 EPNdB footprint area is shown in figure 21. The nozzle

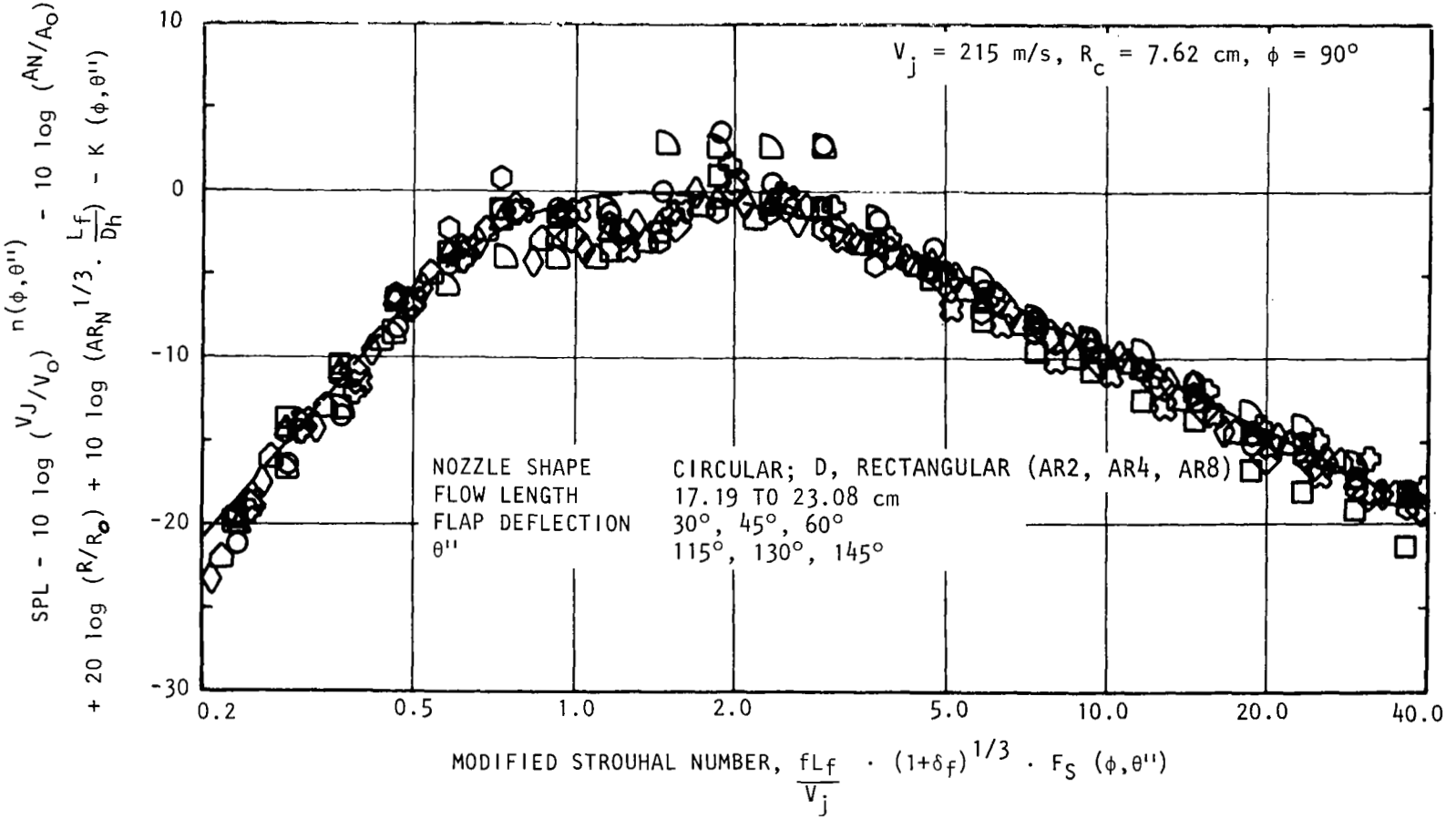

Figure 18. Unified Spectrum Shape for USB Noise Formulation

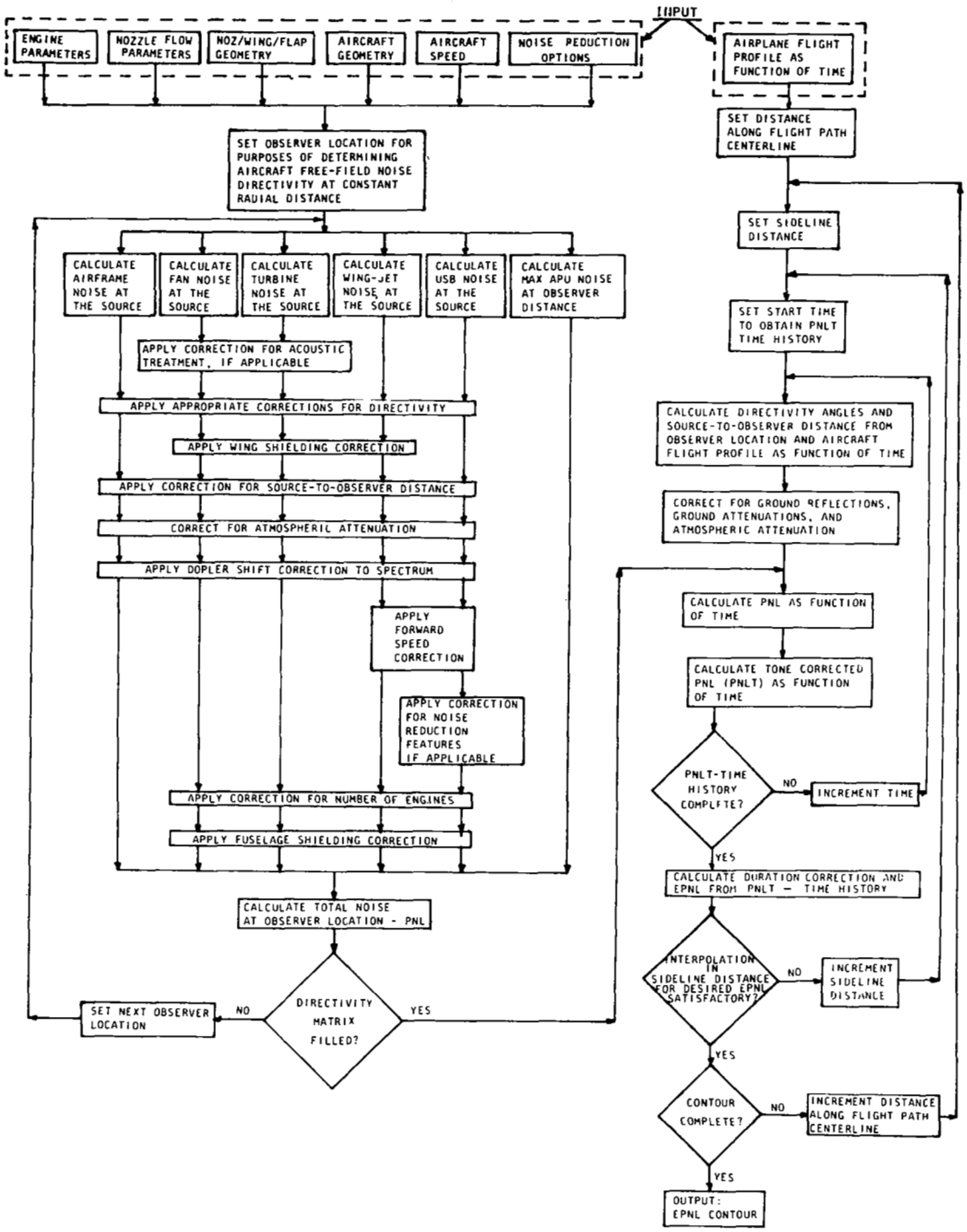

Figure 19. Flow Chart of Noise Footprint Prediction Program

AIRCRAFT NO. →	1	2	3	4	5	6	7	8
MISSION								
NO. OF PASSENGERS	148							
STAGE LENGTH, Km (N.M.)	927 (500)				2780 (1500)			
FIELD LENGTH, m (Ft)	610 (2000)				1219 (4000)			
CRUISE MACH NO.	0.70	0.75	0.80	0.75	0.70	0.75	0.80	0.70
CRUISE ALTITUDE, m (Ft)	9144 (30000)							
PROPULSION SYSTEM								
NOZZLE SHAPE	D (SEMICIRCULAR)				CIRCULAR			
NACELLE TYPE	BLENDED				PYLON-MOUNTED			
NO. OF ENGINES	4				2			
FAN PRESSURE RATIO	1.35			1.47	1.47			1.35
RATED THRUST, N (Lb)	79993 (17984)	83200 (18705)	90753 (20403)	101307 (22776)	160978 (36191)	160946 (36184)	183395 (41231)	203447 (45739)
NACELLE DIAMETER, m (Ft)	2.05 (6.72)	2.09 (6.85)	2.18 (7.15)	2.14 (7.02)	2.70 (8.85)	2.70 (8.85)	2.88 (9.45)	3.26 (10.71)
AIRCRAFT								
RAMP WEIGHT, Kg (Lb)	66266 (146116)	66067 (145678)	68765 (151626)	72563 (160001)	78893 (173959)	80728 (178006)	85544 (188625)	83511 (184141)
WING AREA, m^2 (Ft^2)	186.1 (2003)	169.8 (1828)	159.0 (1711)	199.9 (2152)	172.9 (1861)	185.3 (1995)	169.9 (1829)	204.1 (2197)
WING LOADING, Kg/m^2 (Lb/Ft^2)	354 (72.5)	387 (79.2)	430 (88.0)	359 (73.6)	453 (92.8)	433 (88.6)	499 (102.3)	407 (83.3)
THRUST-TO-WEIGHT RATIO	0.460	0.480	0.503	0.536	0.391	0.382	0.410	0.464
ASPECT RATIO	10.0				7.73			
SWEEP ANGLE, 0.25c, DEGREES	20							
TAPER RATIO	0.3							
THICKNESS RATIO, AVG.	0.141		0.123	0.141	0.141		0.123	0.141
CRUISE DATA								
F_N/MAX CRUISE	1.000			0.600	0.890	0.975	1.000	1.000
C_L	0.325	0.310	0.304	0.291	0.415	0.344	0.350	0.372
C_D	0.0273	0.0256	0.0248	0.0204	0.0335	0.0284	0.0303	0.0317
L_D	11.9	12.1	12.3	14.2	12.4	12.1	11.5	11.7
NACELLE C_D, TOTAL	0.0104	0.0096	0.0096	0.0050	0.0116	0.0096	0.0120	0.0132
TAKEOFF AND LANDING DATA								
CLIMBOUT ANGLE	14.2	14.8	15.5	18.3	11.4	11.2	11.7	14.0
CLIMBOUT SPEED, Km/Hr (Kt)	184.7 (99.6)	184.7 (99.6)	185.4 (100.0)	187.6 (101.2)	250.8 (135.3)	250.5 (135.1)	252.0 (135.9)	228.8 (123.4)
APPROACH ANGLE, DEGREES	5.9	5.9	5.9	6.1	3.8	3.8	3.8	3.6
APPROACH SPEED, Km/Hr (Kt)	160.7 (86.7)	160.2 (86.4)	159.4 (86.0)	153.9 (83.0)	250.5 (135.1)	251.6 (135.7)	247.9 (133.7)	262.9 (141.8)
RATE OF SINK, m/S (Ft/Min)	4.57 (900)							
APPROACH F_N/TAKEOFF F_N	0.38	0.42	0.47	0.45	0.20	0.19	0.24	0.12
COSTS (1972 $)								
ENGINES	$3.59M	$3.64M	$3.75M	$2.83M	$2.08M	$2.08M	$2.18M	$3.11M
COMPLETE AIRCRAFT	$10.58M	$10.82M	$11.34M	$10.36M	$9.49M	$9.80M	$10.44M	$11.15M
DOC, 2 x 1972 FUEL PRICE (23¢/Gal), ¢/SEAT-S.M.	2.33	2.26	2.27	2.27	1.74	1.72	1.76	1.94
DOC, 4 x 1972 FUEL PRICE (46¢/Gal), ¢/SEAT-S.M.	2.94	2.36	2.89	2.99	2.32	2.32	2.40	2.52
NOISE								
TAKEOFF FOOTPRINT, 90 EPNdB, Km^2 ($S.M.^2$)	2.83 (1.09)	3.03 (1.17)	3.47 (1.34)	9.90 (3.82)	15.20 (5.87)	14.66 (5.66)	17.35 (6.70)	4.07 (1.57)
TAKEOFF FLYOVER AT 6.49 Km (3.5 N.M), EPNdB	83.4	83.4	83.7	88.6	95.8	95.6	96.5	85.6
TAKEOFF, MAXIMUM AT 152.4 M (500 Ft), SIDELINE, EPNdB	99.1	99.1	100.3	106.3	106.4	106.2	107.4	101.4
LANDING FOOTPRINT, 90 EPNdB, Km^2 ($S.M.^2$)	0.11 (0.04)	0.18 (0.07)	0.36 (0.14)	1.14 (0.44)	0.11 (0.04)	0.11 (0.04)	0.16 (0.06)	0.11 (0.04)
LANDING FLYOVER AT 1.86 Km (1 N.M.), EPNdB	86.8	88.7	91.1	95.0	86.1	85.9	88.5	85.5
TOTAL FOOTPRINT, 90 EPNdB, Km^2 ($S.M.^2$)	2.94 (1.13)	3.21 (1.24)	3.83 (1.48)	11.04 (4.26)	15.31 (5.91)	14.77 (5.70)	17.51 (6.76)	4.18 (1.61)

Table 2. USB Study Aircraft

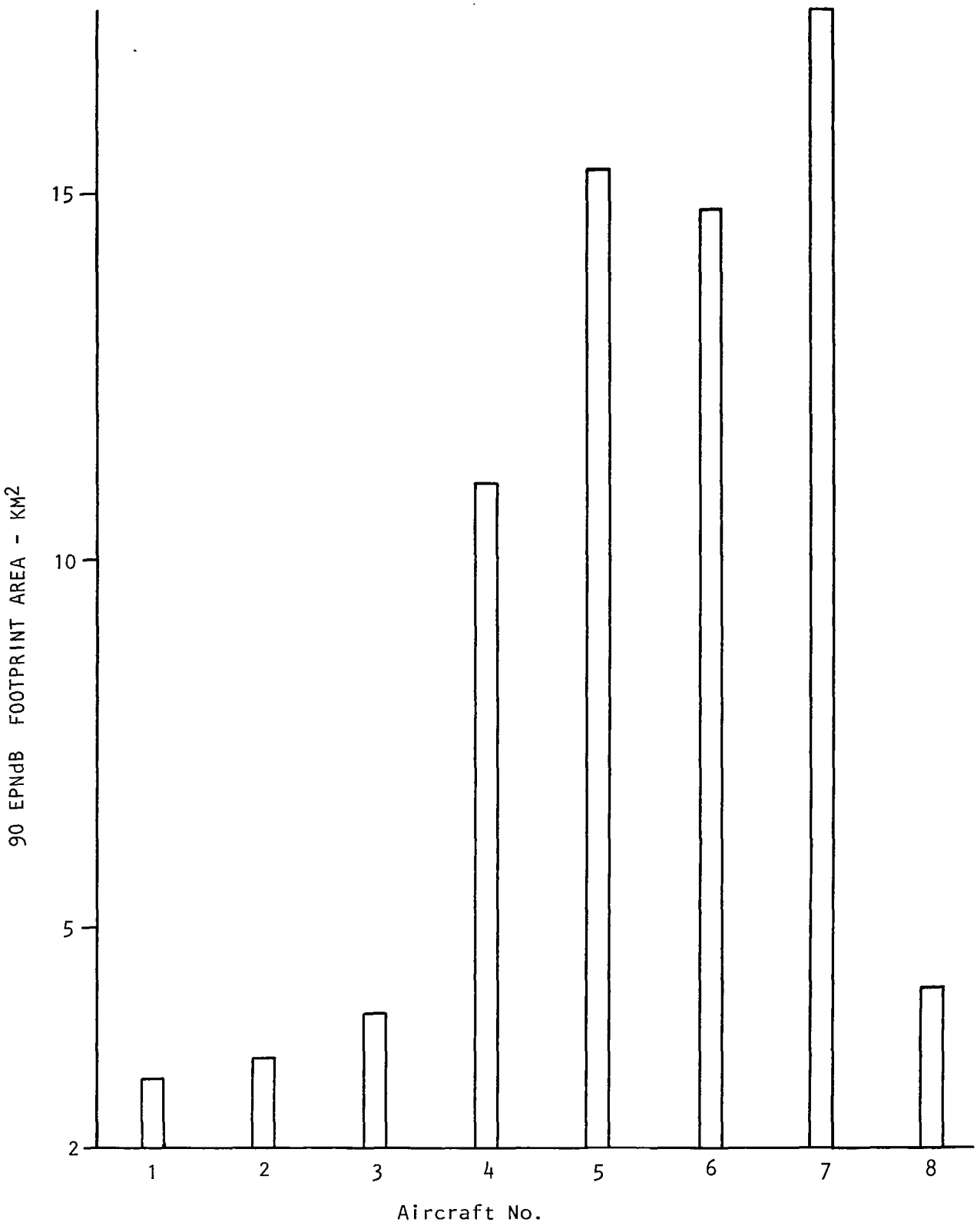

Figure 20. Noise Footprint Areas, USB Study Aircraft

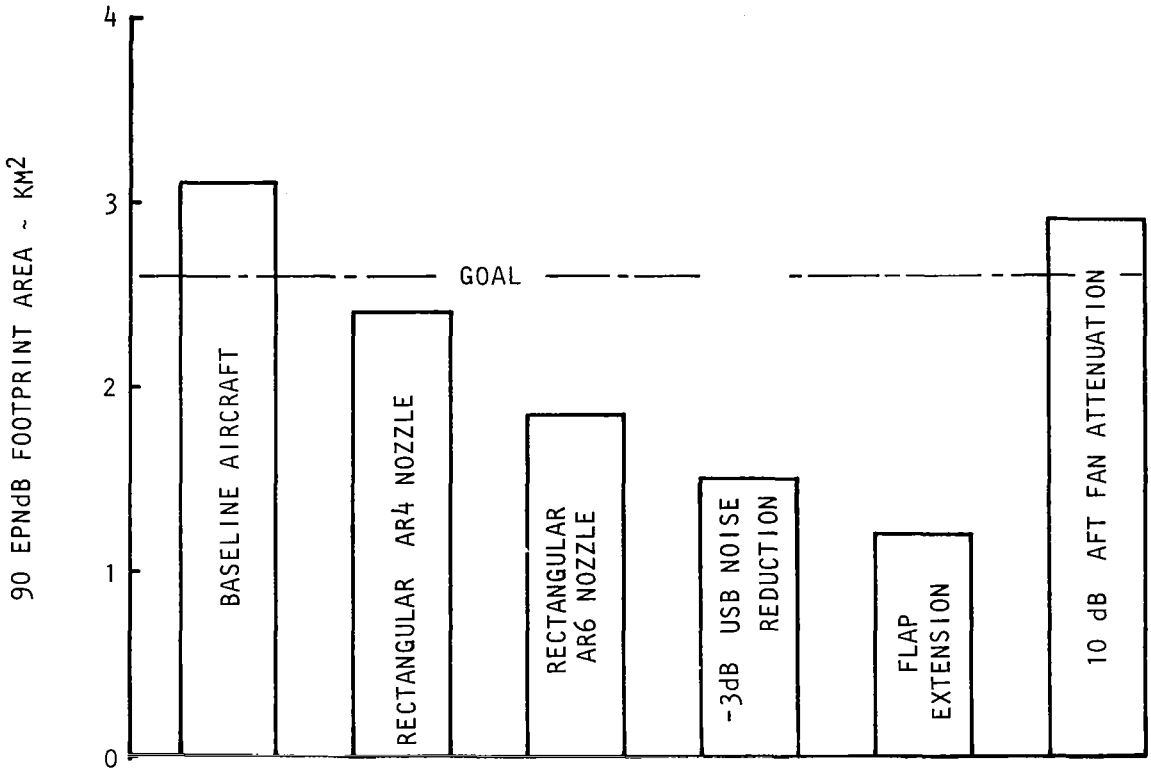

Figure 21. Effect of Some Variables on the Takeoff Noise Footprint Area

aspect ratio and the flap length are shown to be important basic design parameters which affect noise. The use of an aspect ratio 6 nozzle reduced the 90 EPNdB footprint area to 1.8 km^2. Extension of the flap so that the total wing/flap chord was increased by 50% reduces the takeoff footprint area to 1.2 km^2.

Final design. - Based on these studies, the final design shown in figure 22 was evolved. It is very similar to the baseline aircraft: a high-wing four-engine aircraft with a 148-passenger capacity, field length of 610 m, stage length of 927 km, and cruise Mach number of 0.75. The wing area is 170 m^2 with a wing loading of 387 kg/m^2. The 1.35 fan pressure ratio engines are scaled to a takeoff rated thrust of 83,200 N, which gives a thrust-to-weight ratio of 0.48. The approach speed is 160 km/hr and climbout speed is 185 km/hr. The nacelle has a D nozzle located at 35% chord with a boattail angle of 16°. Extended-chord flaps are used to get the noise benefit of the increased flow length from the nozzle to the trailing edge, and the flap internal blowing system used in the baseline configuration is deleted. The aft fan duct noise treatment was found to be not necessary, although there is provision to incorporate treatment both in forward and aft directions.

Separation of the fan and primary duct flow streams is maintained right up to the nozzle discharge in order to minimize flow separation and other interaction effects. The primary nozzle is slightly S-shaped in the side view but a circular cross-section is maintained throughout. The design incorporates steel honeycomb sandwich with the forward inner portion fabricated to include a perforated face sheet to attenuate turbine noise. The outer fan duct above the wing surface is conventional sheet metal/stiffener construction.

A long chord, high-extension flap system was selected. Directly behind the engine, the flap surface is continuous, as is shown in figure 23. The flap system shown indicates how the chord extension can be obtained. The first flap segment slides back on a fixed track. The second segment is mounted to the first through another track which provides further extension. As shown in a representative landing configuration, the extension, measured

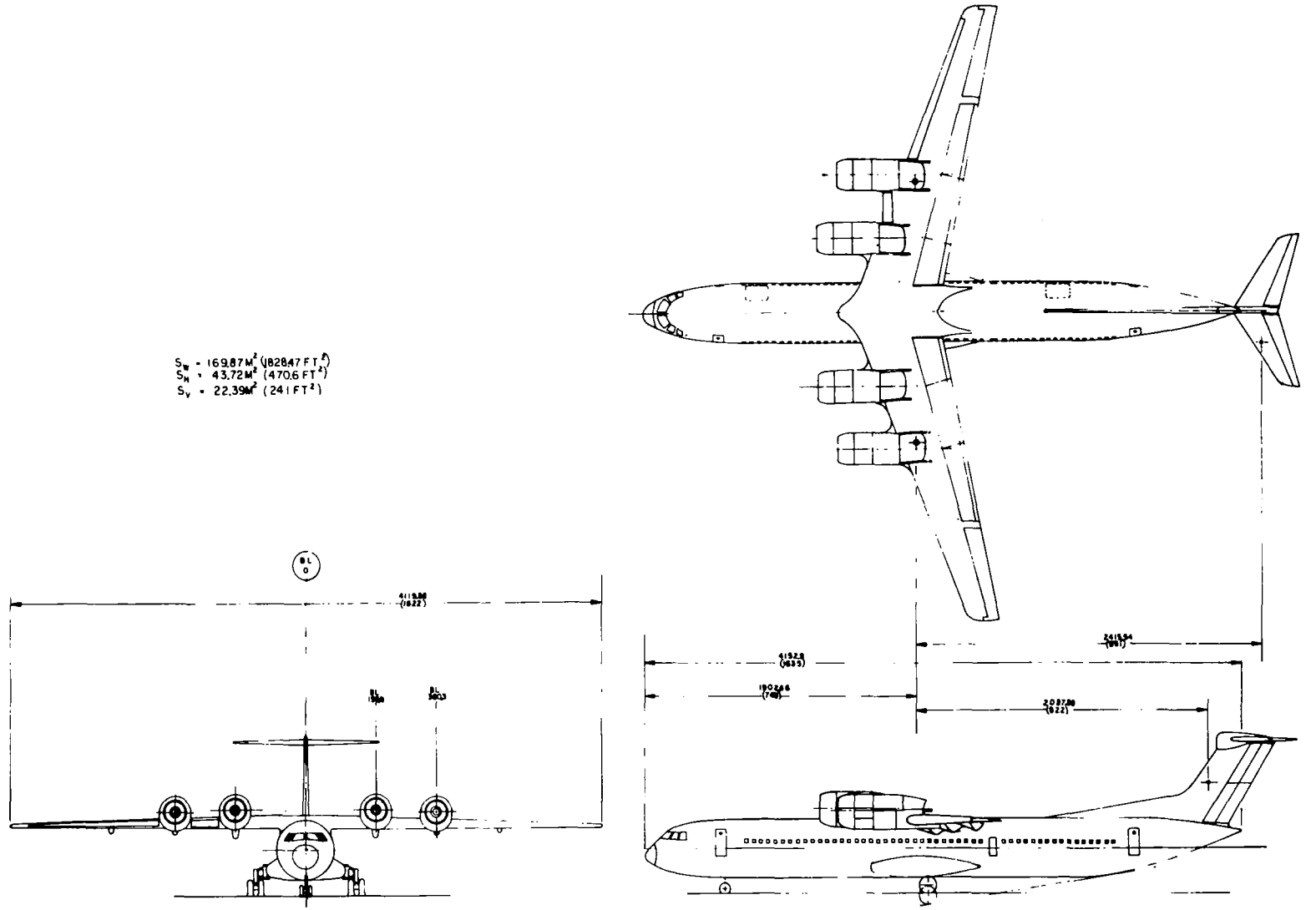

Figure 22. General Arrangement, Baseline Aircraft

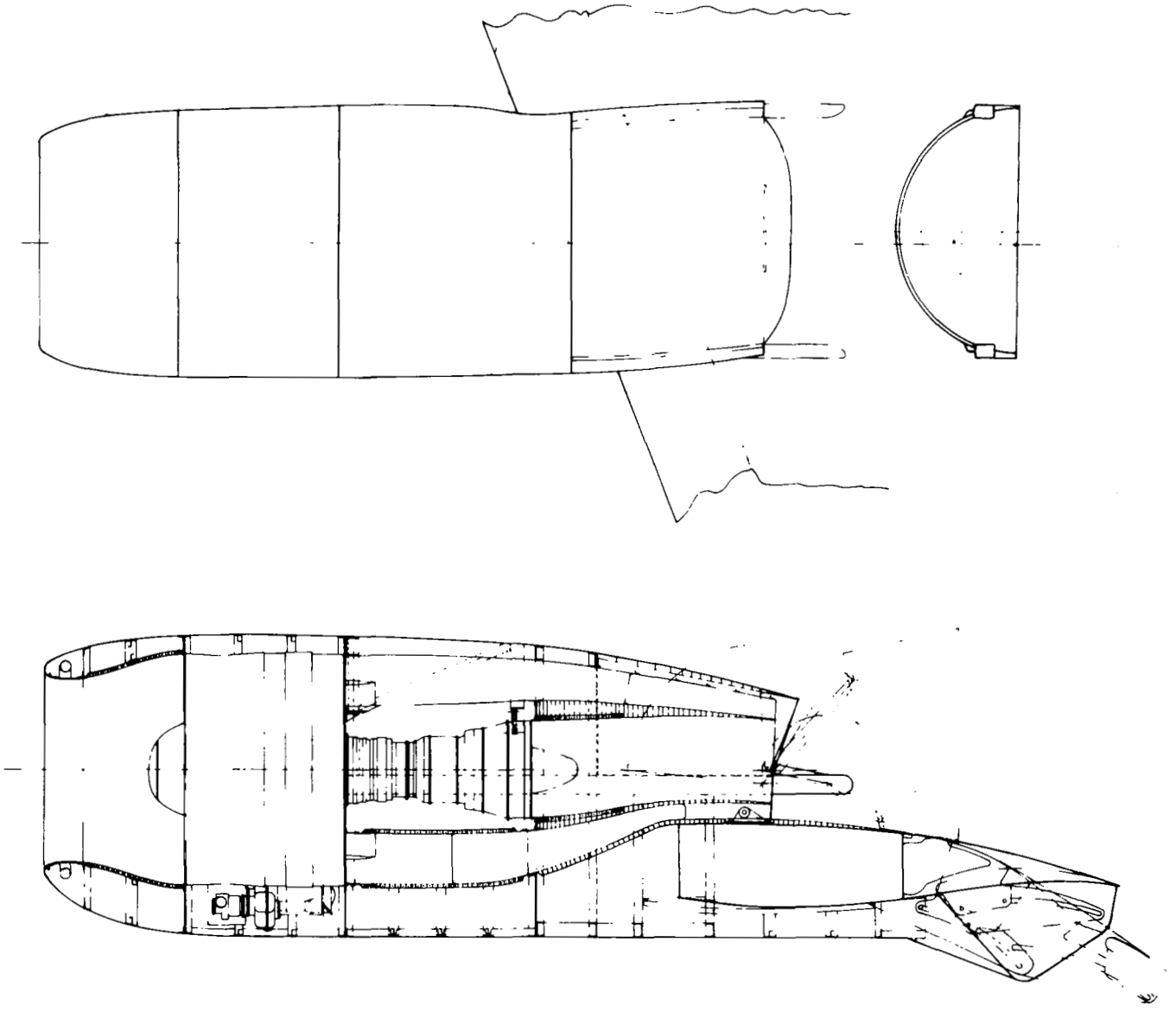

Figure 23. Nacelle Inboard Profile

along the upper surface, is 36% of the wing chord. At takeoff the extension with this track configuration would be about 25% of the wing chord. It is expected that the flap system shown in figure 23 could be modified to provide a 40% chord extension both during takeoff and landing.

Noise. - The flight path and footprint calculated for the final design aircraft are shown in figure 24. The total 90 EPNdB footprint area is 1.83 km^2, considerably below the goal of 2.59 km^2. Typical takeoff spectra of the various noise sources considered in the prediction program and of the complete aircraft are presented in figure 25.

THEORETICAL DEVELOPMENTS

It has been suggested from previous experimental and analytical investigations that the flow mixing noise downstream of the trailing edge is the dominant noise source in practical USB flap systems. Therefore, a theory was developed for the radiated noise generated in the highly sheared layer of the trailing edge wake of USB flaps. The following assumptions were made in developing the relation between the flow characteristics and the radiated sound field.

1. The wake is locally two dimensional with constant thickness, δ.

2. Turbulence is spatially homogeneous with respect to any plane parallel to the shear layer.

3. The fluid inside the layer is assumed to be incompressible.

The fluctuating pressures in the shear layer due to turbulence are given by the solution of Poisson's equation. The details of these theoretical developments are presented in reference 2.

Considering only the components of fluctuating pressures with supersonic phase velocity, the radiated sound is derived using the wave equation. With reasonable approximations, the sound power radiated per unit frequency per

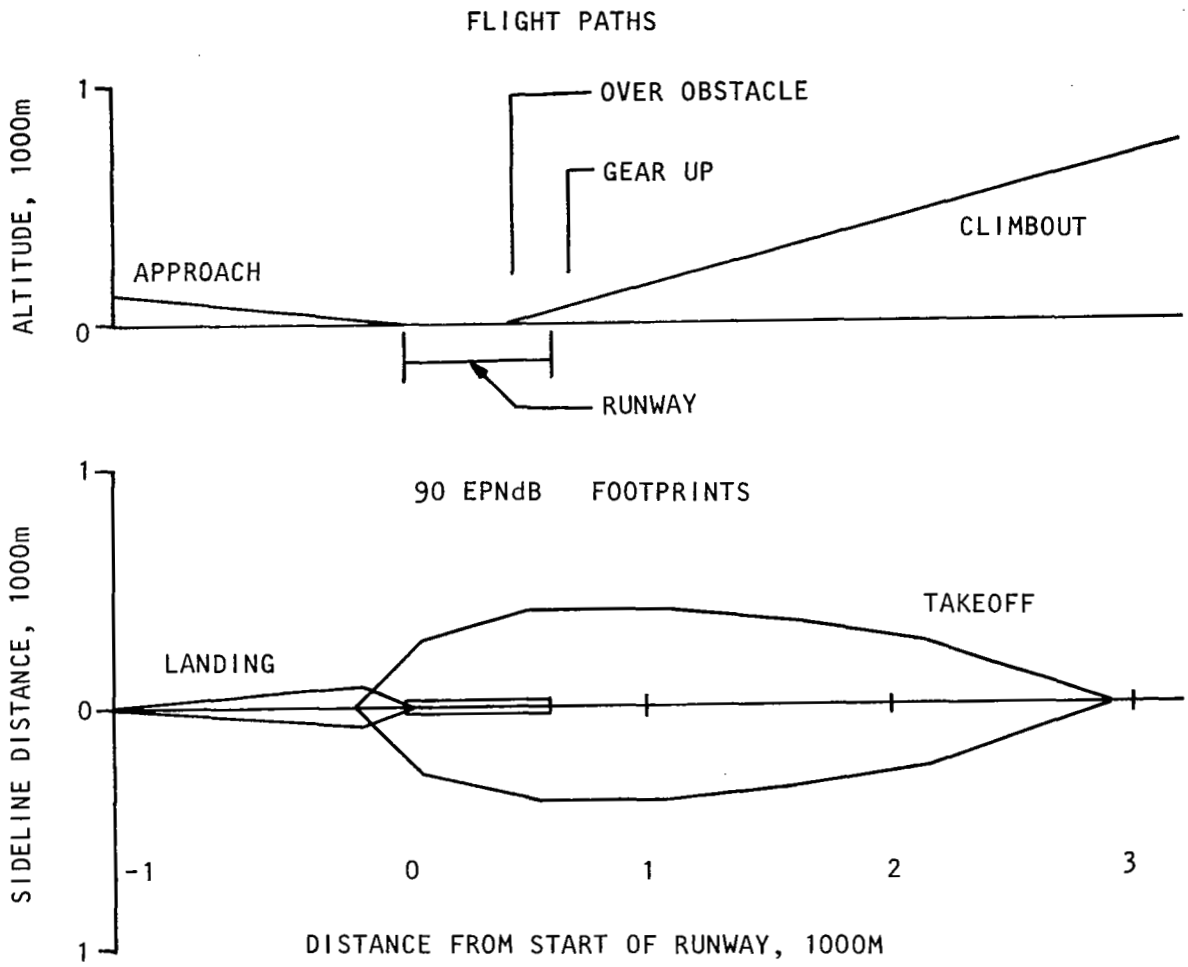

Figure 24. Flight Paths and Noise Footprints, Final Design Aircraft

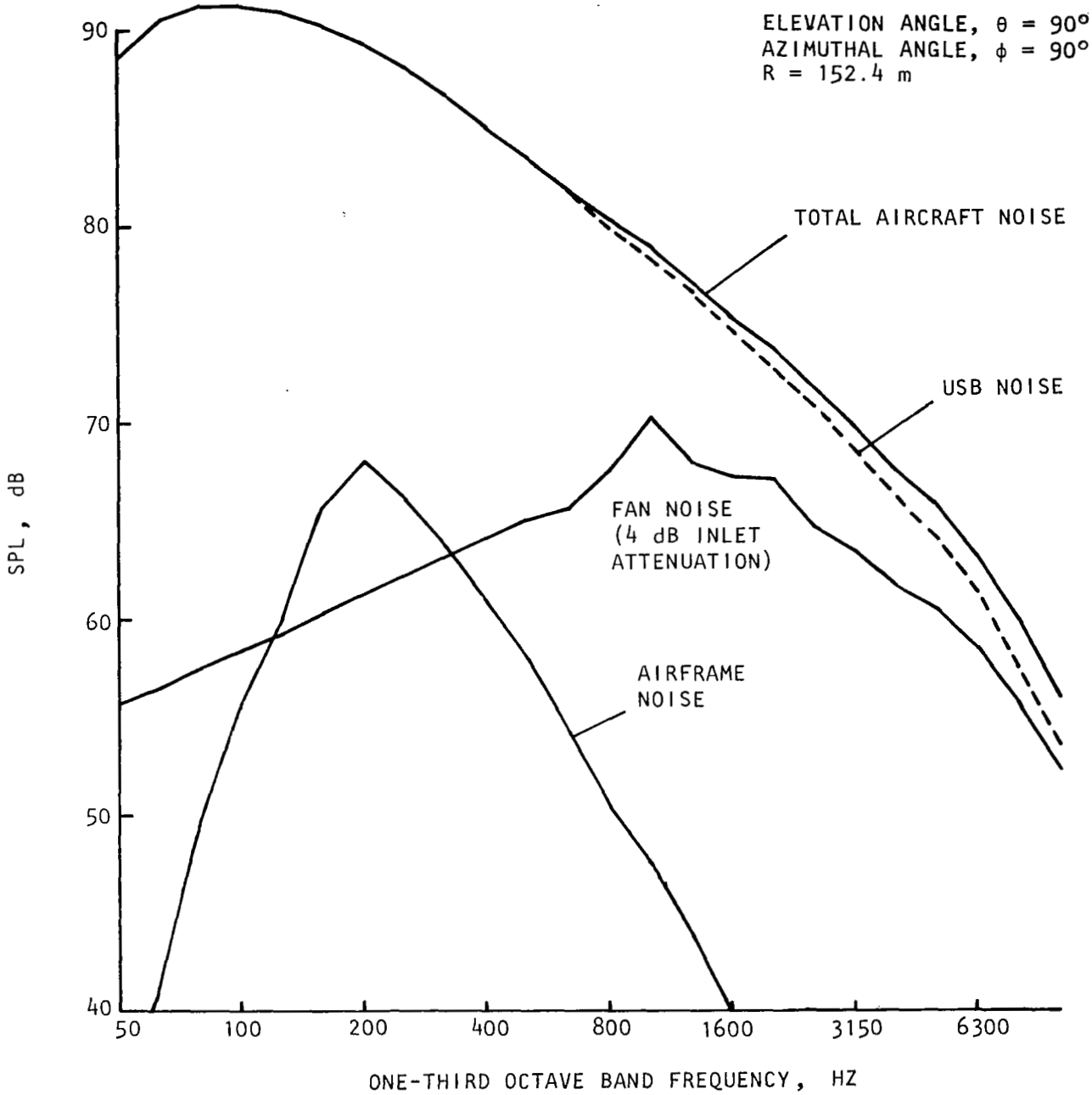

Figure 25. One-Third Octave Band Spectra for Baseline Aircraft (Takeoff condition)

unit solid angle from a unit surface of the shear layer in the direction from the shear layer is given by the directivity function, $D(\psi,\omega)$ as,

$$\frac{D(\psi,\omega)}{\rho U^2 \delta} = \frac{\frac{U_c}{U}\left(\frac{\omega\delta}{U}\right)^2 M^3 \sin\psi}{2\pi^2\beta\lambda}$$

$$\frac{\sum_{i=1}^{N} A_i\alpha_i K_o\left(\frac{\alpha_i\omega\delta}{U}\right)\left[\frac{1}{U^4}\iint_{-\delta}^{o}\frac{d\bar{u}}{dz'}\frac{d\bar{u}}{dz''}G(z',z'')\,dz'\,dz''\right]}{\sum_{i=1}^{N}\left[\left(\frac{A_i}{\alpha_i}\right)\frac{1}{\lambda^2}+\left(\frac{\omega\delta}{U}\right)^2\left(M\cos\psi-\frac{U}{U_c}\right)^2\right]} \qquad (3)$$

For a fixed Strouhal number, $S=\omega\delta/U$, the quantities in square brackets are not expected to be strongly dependent on U. To obtain the total noise radiation in a fixed direction, it is necessary to integrate the above expression over the whole surface of the turbulent shear layer. If L_s is the effective length of this surface area, then the product $L_s\delta$ is weakly dependent on U. Therefore, this equation suggests that the trailing edge noise per unit frequency is roughly proportional to U^5 (or U^6 dependence for total noise power).

Comparison of theory with experimental data. In order to compare the theoretical results with measured data, the equation is rewritten in the following simplified form:

$$D(\psi,\omega) = C\,\omega^2\sin\psi\cdot\frac{\sum_{i=1}^{3} A_i\alpha_i K_o\left(\frac{\alpha_i\delta\omega}{U}\right)}{(\lambda\delta)^{-2}+\left(\frac{\omega}{U}\right)^2\left(M\cos\ -\frac{U}{U_c}\right)^2} \qquad (4)$$

where

$$C = \frac{\rho U_c}{2\pi^2\,U^2a^2\beta\lambda\sum_{i=1}^{3}\frac{A_i}{\alpha_i}}\iint_{-\delta}^{o}\frac{d\bar{u}}{dz'}\frac{d\bar{u}}{dz''}\,G(z',z'')\,dz'\,dz''$$

The unknowns in this equation, A_i, $\alpha_i\delta$, and U_c/U which describe the flow characteristics in the trailing edge wake were not available for a general configuration. Therefore, these quantities were determined from the measured turbulence data of this program. The following values were derived and used:

$A_1 = 0.7$	$A_2 = 6.3$	$A_3 = 3.0$
$\alpha_1\delta = 0.256$	$\alpha_2\delta = 1.12$	$\alpha_3\delta = 16.0$
$U_c/U = 0.9$	$\lambda\delta = 2.84$	

Once the value of C is chosen, however, the sound pressure in any direction and at any frequency can be determined (i.e., is independent of frequency and directivity). The experimental data were obtained from the tests of the USB configuration under static conditions (without free flow). A typical comparison of one-third octave band sound pressure levels is shown in figure 26. The directivity pattern of one-third octave band sound pressure levels at center frequencies of 400, 1600, and 8300 Hz are shown in figure 27. From these figures it may be seen that there is very favorable agreement over most of the spectrum in all directions.

This analysis was developed for the noise generated by the turbulent flow mixing downstream of the trailing edge of a practical USB configuration. Since these calculated results compare well with the measured USB noise data below the wing, it may be concluded that the noise generated downstream of the trailing edge is the dominant source. These results also indicate that the sound field radiated below the wing is primarily a function of the flow parameters in the trailing edge wake. At the present time, no analytical or experimental data are available to relate the trailing edge wake properties to the configuration geometric and operational parameters. Therefore, additional work is necessary to extend this theory to be used in a practical noise prediction program.

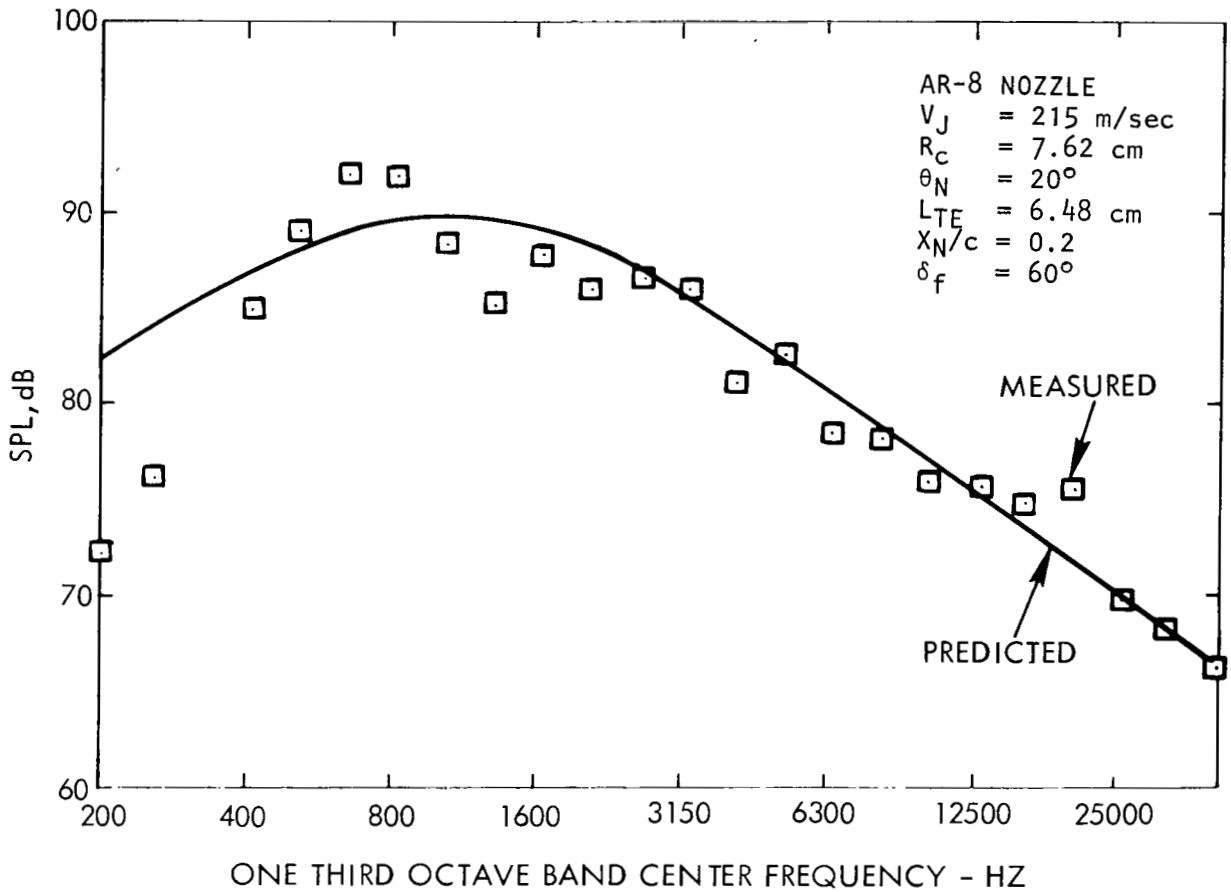

Figure 26. Comparison of Measured Spectra With the Theoretical Prediction

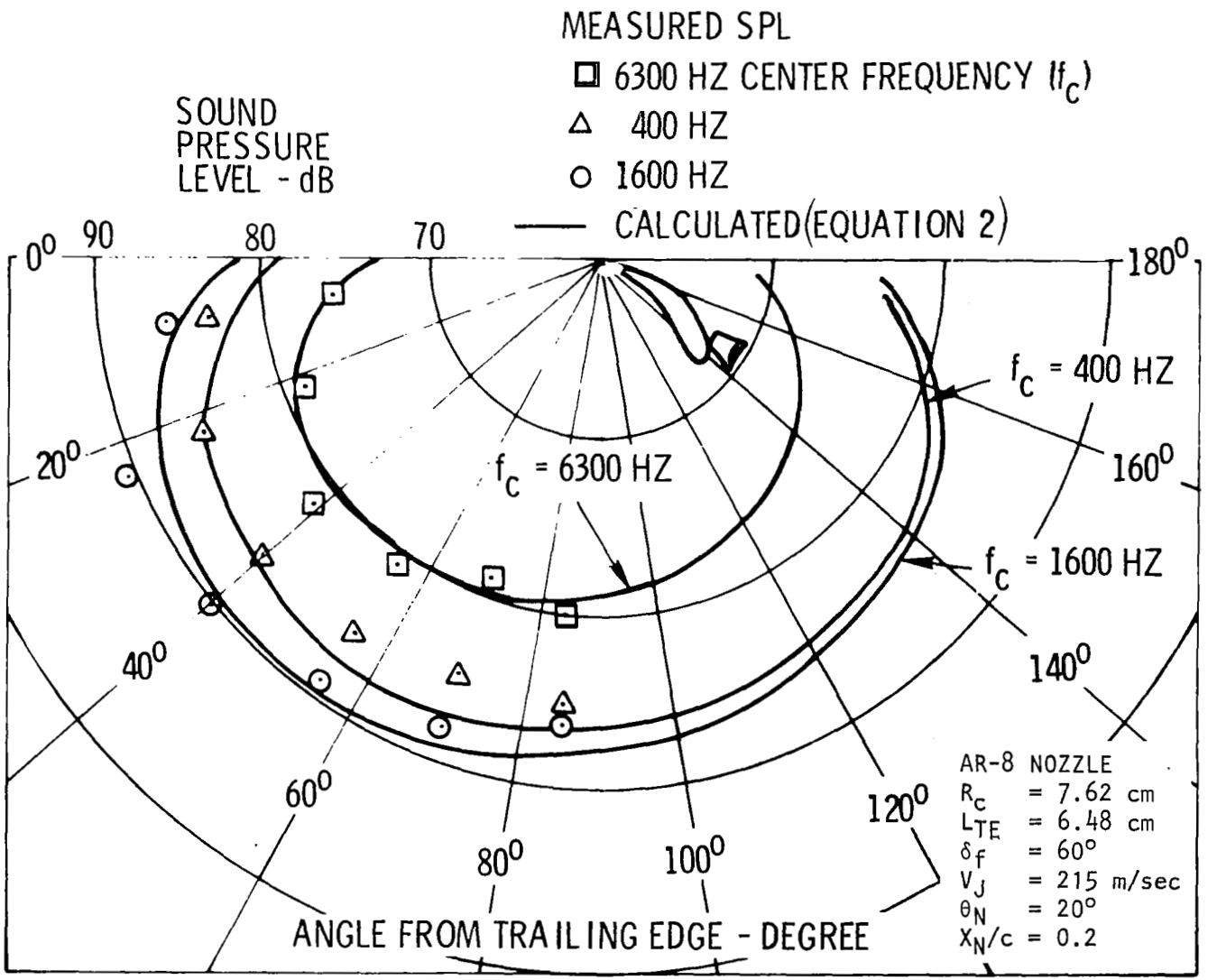

Figure 27. Comparison Between Calculated and Measured Sound

CONCLUSIONS

Experimental and theoretical studies were conducted to develop a noise data base for USB integrated powered-lift systems. The following major conclusions are drawn from these investigations.

1. For a practical upper-surface blown flap configuration, the turbulent mixing just downstream of the trailing edge is the dominant noise source from the community noise point of view.

2. The far-field sound of USB is primarily a function of the flow parameters in the trailing edge wake. These parameters are primarily functions of jet exit velocity.

3. Turbulence intensity in the trailing edge wake can be decreased by increasing the nozzle impingement angle and flow length. This reduction in turbulence tends to reduce the radiated noise.

4. The ratio of flow path length to the hydraulic diameter of the nozzle appears to be a good parameter to describe the flow characteristics at the trailing edge and the radiated noise characteristics.

5. The nozzle shape has some influence on the radiated noise, particularly in the mid frequencies. As the nozzle aspect ratio increases, the noise levels decrease, because of improved flow spreading on the flap surface.

6. For geometrically similar models, the noise data can be scaled by assuming the sound pressure is directly proportional to the nozzle exit area and the frequency is inversely proportional to the square root of the nozzle area.

7. In addition to jet velocity, the flow path length and the flow direction in the trailing edge wake are the important parameters controlling the noise characteristics.

8. One of the ways of reducing radiated noise is to modify the wake shear layer so that the turbulence generation is reduced. Secondary blowing from a slot on the upper surface just upstream of the flap trailing edge is such a modifier and appears to have potential for reducing USB noise.

9. Forward speed generally decreases low-frequency noise. It has little effect at the high frequencies at most locations, but causes an increase in high frequency noise at the extreme aft quadrant (behind the wing).

10. USB noise levels predicted using the empirical method compare favorably with various available static test data.

11. USB aircraft design studies were conducted using the empirical noise prediction program. Cruise performance was calculated using the recent data base developed at Lockheed under NASA Contract No. NAS1-13871. Design studies indicate that by incorporating a jet exhaust nozzle with an aspect ratio of 4 or 6 and an extended flap, a practical USB aircraft can have a 90 EPNdB footprint area as small as 1.2 km^2. This design is compatible with acceptable aero-propulsion performance requirements.

12. The noise characteristics predicted using the theoretical model for trailing edge noise compared rather favorably with measured data. However, further developments of the theory are necessary in order for it to be generally useful in USB noise prediction.

REFERENCES

1. Brown, W. H.; Searle, N.; Blakney, D. F.; Pennock, A. P.; and Gibson, J. S.: Noise Characteristics of Upper Surface Blown Configurations; Experimental Program and Results. NASA CR-145143, October 1977.

2. Reddy, N. N.; Pennock, A. P.; Tibbetts, J. G.; and Tam, C. K. W.: Noise Characteristics of Upper Surface Blown Configurations – Analytical Studies. NASA CR-2812, March 1978.

3. Heidelburg, L. J., et al.: Full-Scale Upper-Surface-Blown Flap Noise. SAE Paper 750609, May 1975.

4. Falarski, M. D., et al.: Acoustic Characteristics of a Large-Scale Wind Tunnel Model of an Upper-Surface Blown Flap Transport Having Two Engines. NASA TMX-62319, Sept. 1973.

5. Reshotko, M., et al.: Engine-Over-the-Wing Noise Research. NASA TMX-68246, July 1973.

1. Report No.	2. Government Accession No.	3. Recipient's Catalog No.
NASA CR-2918		

4. Title and Subtitle	5. Report Date
NOISE CHARACTERISTICS OF UPPER SURFACE BLOWN CONFIGURATIONS - SUMMARY	June 1978
	6. Performing Organization Code
7. Author(s)	8. Performing Organization Report No.
N. N. Reddy and J. S. Gibson	LG77ER0103
	10. Work Unit No.
9. Performing Organization Name and Address	11. Contract or Grant No.
Lockheed-Georgia Company Marietta, Georgia	NAS1-13870
	13. Type of Report and Period Covered
12. Sponsoring Agency Name and Address	FINAL REPORT May 1975 - Nov. 1976
National Aeronautics and Space Administration Washington, D. C. 20546	14. Sponsoring Agency Code

15. Supplementary Notes

Contract Monitor - W. C. Sleeman, Jr., NASA Langley Research Center
Hampton, Virginia 23665
Program Manager - J. S. Gibson, Lockheed-Georgia Comapny, Marietta, Georgia 30063

16. Abstract

A systematic experimental program was conducted to develop a data base for the noise and related flow characteristics of upper surface blown configurations. The effect of various geometric and flow parameters was investigated experimentally. The dominant noise was identified from the measured flow and noise characteristics to be generated downstream of the trailing edge. The possibilities of noise reduction techniques were explored. A USB noise prediction program was developed empirically to calculate noise levels at any point and noise contours (footprints). Using this noise prediction program, and the cruise performance data base from NASA Contract NAS1-13871, aircraft design studies were conducted to integrate low noise and good performance characteristics. A theory was developed for the noise from the highly sheared layer of a trailing edge wake. Theoretical results compare favorably with the measured noise of the USB model.

17. Key Words (Suggested by Author(s))	18. Distribution Statement
USB Noise, STOL Noise, Noise Characteristics, Noise Prediction, Trailing Edge Noise, Noise Reduction, Flow Characteristics	Unlimited Subject Category 71

19. Security Classif. (of this report)	20. Security Classif. (of this page)	21. No. of Pages	22. Price*
UNCLASSIFIED	UNCLASSIFIED	59	$5.25

* For sale by the National Technical Information Service, Springfield, Virginia 22161

NASA-Langley, 1978